

Impact of Interatomic Electronic Decay Processes on the Width of the Xe $4d$ Lines in the Auger Decay of the Xenon Fluorides

Christian Buth,^{*} Robin Santra,[†] and Lorenz S. Cederbaum

Theoretische Chemie, Physikalisch-Chemisches Institut, Ruprecht-Karls-Universität Heidelberg, Im Neuenheimer Feld 229, 69120 Heidelberg, Germany

(Dated: March 19, 2003)

For a long time, the Auger effect in molecules has been thought of to be an intra-atomic process, involving mainly the molecular orbitals with a high probability amplitude on the atom which carries the initial vacancy. Newer investigations suggest that this picture fails for certain molecules. We investigate the Auger decay of Xe $4d$ -ionized xenon fluorides (XeF $_n$, $n = 2, 4, 6$) with respect to the recently discovered interatomic electronic decay processes *interatomic Coulombic decay* (ICD) and *electron transfer mediated decay* (ETMD). It is shown that the broadening of the Xe $4d$ line width in XeF $_n$ with increasing n can be attributed to them. The phenomenon of *foreign imaging* is explained in terms of ICD and ETMD.

I. INTRODUCTION

The Auger effect¹⁻⁵ has provided a magnificent means to study atoms, molecules and surfaces. It is caused by a special type of electronic resonance, i.e. the decay by electron emission of core-ionized atoms or molecules and it has received much attention since its discovery because it is a fundamental process which yields deep insights into complex many-body effects in atoms and molecules. The Auger effect has proven to be useful in many experimental situations²⁻⁶ and can be used as an analytical tool. Therefore an in depth understanding of the Auger effect is important both for fundamental and for practical reasons. Over the years there were many attempts to calculate Auger decay rates and as soon as Auger transitions involving valence orbitals in molecules came into the focus of interest the question of the importance of interatomic transitions arose⁶ and is still by far not completely elucidated. Matthew and Komminos were the first to examine interatomic Auger transition rates⁷. Using too strong approximations⁶ they falsely concluded that these transitions have a small impact on the Auger rate, except in low energy Auger processes. Recent theoretical and experimental investigations show that the effect of the chemical bond can be dramatic⁸⁻¹².

Clusters¹³ of atoms or molecules have been receiving much attention because they can be seen as a bridge between the individual monomer and the condensed phase formed by many monomers. They also provide ideal examples to investigate the role of interatomic (intermolecular) decay processes. In clusters new interatomic and intermolecular electronic decay processes were discovered recently that basically involve neighboring atoms¹⁴⁻¹⁹ and that do not take place in the individual monomer. Since the understanding of these processes is essential for this work, these processes will be briefly described in the following section II. Evidence for the new interatomic decay processes predicted theoretically has been found recently²⁰ in neon clusters with the help of photoelectron spectroscopy. In this work we investigate the role of these processes in the Auger decay in molecules. Gen-

eral aspects are discussed and exemplified for XeF $_n$, $n = 0, 2, 4, 6$. The XeF $_n$ constitute an ideal example because of the weak bonding between the central noble gas atom and the fluorine atoms allowing us to identify various interatomic processes and to discern them from intra-atomic ones. Here, we would like to draw the reader's attention to the recent interesting experimental study and its analysis on SiF $_4$ ¹².

Photoelectron spectroscopy was used to examine the Xe $4d$ lines in the xenon atom and in the xenon fluorides (XeF $_n$, $n = 2, 4, 6$)²¹. In figure 1 the line width of the Xe $4d$ lines is plotted for all these systems^{21,22}. The graph suggests that the line width of the compounds increases with an increasing number of fluorine atoms. Several experimental line widths are measured for each compound which originate from the decay of the initial ionization of the non-equivalent Xe $4d$ orbitals.

The observed increase in line width raises the question whether the increase may be caused by an increased electronic decay rate, or whether it is caused by, e.g., unresolved vibrational broadening²¹. Cutler *et al.* reason that vibrational broadening does not lead to a significant effect because in other compounds, e.g. Ge $3d$, this was not important for d -level electrons²¹. Therefore, the electronic decay rate of Xe $4d$ -ionized XeF $_n$ is examined in this work to elucidate which types of electronic decay processes are responsible for the increased line width in XeF $_n$.

To this end, section III introduces a many-body Green's function method, the algebraic diagrammatic construction scheme, to calculate ionization spectra of molecules. A two-hole population analysis^{8,23} serves as an important tool for the analysis of the localization of final states which is used together with Wigner-Weisskopf theory^{24,25} to elucidate the dependence between decay width and final state population numbers. Section IV describes all details involved in the calculation of the ionization spectra of XeF $_n$. The single and double ionization spectra are analyzed in section V and the relevance of interatomic decay processes for the decay of Xe $4d$ vacancies is discussed. Consequences and perspectives of our work for the understanding of molecular Auger decay are

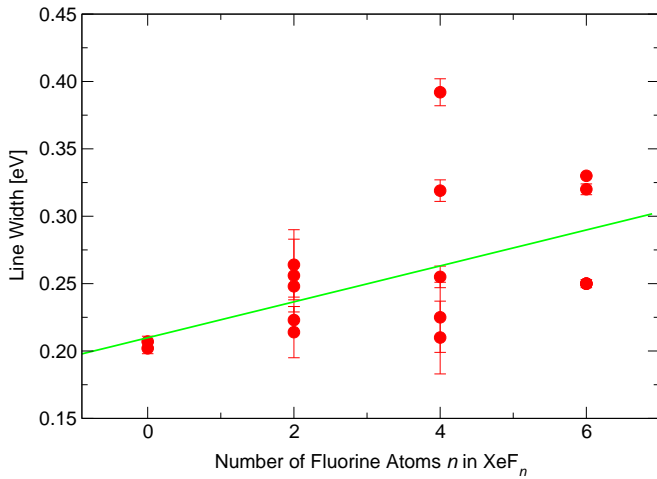


FIG. 1: Experimental widths of the Xe 4d lines in Xe, XeF_2 , XeF_4 and XeF_6 . The figure²² suggests an average increase of the line width with an increasing number of fluorine atoms.

illuminated in section VI.

II. ELECTRONIC DECAY PROCESSES

In this section we present the knowledge obtained in the study of the decay of inner valence ionized clusters of atoms and clusters of molecules clearly and self-contained. We elucidate parallels and draw conclusions for molecular Auger decay. All decays presented here are electronic decays, i.e. an electron is emitted after the initial ionization. For sure, there is always the possibility of a decay by photon emission or dissociation, but lifetime calculations show that the electronic decay is very fast and consequently is the dominant process^{17,19,26–28} for inner valence ionized clusters. This fact is also well known in the case of core hole decay^{2–5}. We mention that the decay processes, discussed below for singly ionized systems, can be generalized to describe the decay of inner valence vacancies of multiply ionized clusters¹⁶.

A. Intra-atomic Electronic Decay

Intra-atomic electronic decay is usually the most prominent electronic decay process of core-ionized molecules or clusters of atoms or molecules and is closely related to the Auger decay¹ in an isolated atom. In atoms this mechanism is well understood^{1–5}: the initial core hole is filled by a (valence) electron and the excess energy is transferred to a second (valence) electron which is emitted subsequently (figure 2). In molecules or clusters of atoms or molecules intra-atomic decay is not the only decay process because other processes can occur which involve neighbor atoms or neighbor molecules.

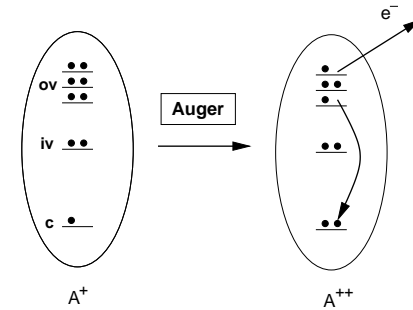


FIG. 2: Principle of Auger decay. The initial core hole is filled by a valence electron. The excess energy is released by emitting a second valence electron. **A**: atom, **ov**: outer valence orbital, **iv**: inner valence orbital, **c**: core orbital.

B. Interatomic and Intermolecular Coulombic Decay

If one removes an inner valence electron from an isolated atom or molecule, in general, it cannot decay by electron emission because it is below the double ionization threshold. The situation changes if the monomer is part of a cluster: the initial inner valence vacancy is filled by a valence electron of the same monomer and the excess energy is transferred to a second valence electron of a neighboring monomer which is emitted subsequently. See figure 3 for a schematic representation.

The repulsion between two holes localized on two different monomers, the so-called *two-site states*, is reduced due to the larger spatial separation of the two final state holes, in comparison to the repulsion between two holes localized on one monomer, the so-called *one-site states*. This increased spatial separation of the final state holes leads to a reduction in energy for two-site states which lowers the double ionization threshold and a decay by electron emission becomes energetically possible.

The decay process is termed *interatomic* or *intermolecular Coulombic decay (ICD)* for clusters of atoms or clusters of molecules, respectively. It was identified in several weakly bound clusters: $(\text{HF})_n$ clusters^{14,16,18}, the $\text{HF}(\text{H}_2\text{O})_2$ cluster²⁹, $(\text{H}_2\text{O})_n$ clusters¹⁴, $(\text{Ne})_n$ clusters^{15,19,30,31}, the NeAr dimer¹⁷ and found to be a very efficient decay. Further we would like to point out Ref. 32 for a study of electronic decay after inner-valence ionization of fluorinated carbanions and their acids.

The ICD decay width in $(\text{Ne})_n$ clusters was found to increase strongly with n where the central neon atom carried the initial inner valence vacancy and the surrounding atoms converged with n to the shape of the first coordination shell in solid neon¹⁹.

C. Electron Transfer Mediated Decay

The ionization spectra of neon and argon are very different (Ref. 17 and references therein), neon has higher

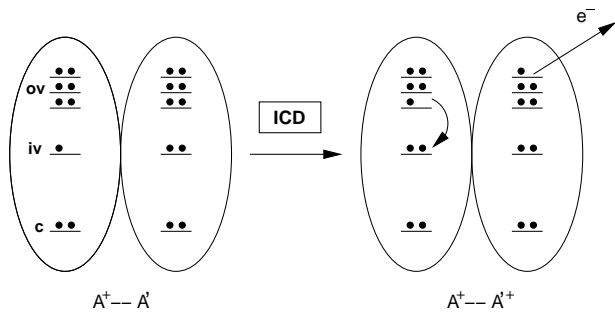


FIG. 3: Principle of interatomic or intermolecular Coulombic decay. The initial inner valence vacancy is filled by a valence electron of the same monomer. The excess energy is released by emitting a second valence electron of a neighboring monomer. **A**, **A'**: atoms, **ov**: outer valence orbital, **iv**: inner valence orbital, **c**: core orbital.

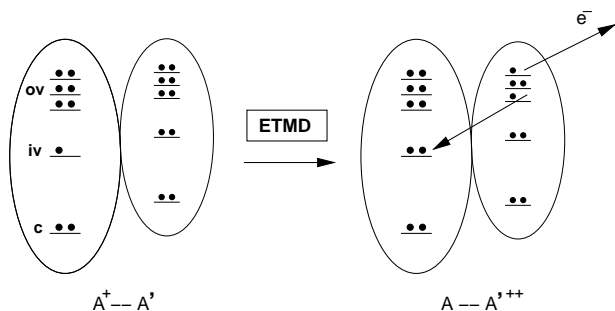


FIG. 4: Principle of two-monomer electron transfer mediated decay. A valence electron of A' drops into the hole on A and the excess energy is transferred to another valence electron of A' which is emitted subsequently. **A**, **A'**: atoms, **ov**: outer valence orbitals, **iv**: inner valence orbital, **c**: core orbital. The inner valence IP of A is higher than the double ionization threshold of A' .

lying single ionization potentials (IP) and double ionization potentials (DIP) compared to argon. In fact, the inner valence Ne $2s$ IP is larger than the Ne $^{-1}$ Ar $^{-1}$ DIP in the NeAr dimer¹⁷. [The superscript numbers -1 , -2 denote the number of electrons missing on the atom written to its left (compared to the isolated, neutral atom). This idealized picture assumes a strong localization of the electron vacancies on the atoms.] Therefore, an initial Ne $2s$ vacancy can lead to ICD.

The Ne $2s$ vacancy can decay in another way, too, because the Ne $2s$ IP is also larger than the NeAr $^{-2}$ DIP. In this case, a valence electron from argon drops into the Ne $2s$ hole and the excess energy is transferred to another valence electron of argon which is emitted subsequently, leaving the dimer in a NeAr $^{-2}$ state. This process is called *electron transfer mediated decay (ETMD)*¹⁷. A schematic representation of the ETMD process is shown in figure 4.

In Ref. 17 it is shown that the contribution of ETMD to the total electronic decay width of an initial Ne $2s$ va-

cancy is appreciably smaller compared to the contribution of ICD in NeAr. In the light of the vastly increasing ICD decay width in neon clusters¹⁹ we expect this to hold for ETMD, too. In the ETMD described, only two atoms are involved and, therefore, it is called *two-monomer ETMD*.

In Ref. 17 a *three-monomer ETMD* is suggested to occur for an initial Ne $2s$ vacancy in NeAr $_2$. A schematic representation of this (proposed) process is given in figure 5. A valence electron of the first argon atom drops into the initial Ne $2s$ hole. The excess energy is transferred to a valence electron of the second argon atom which is emitted subsequently, leaving the trimer in a NeAr $^{-1}$ Ar $^{-1}$ state.

D. Self Imaging and Foreign Imaging

This subsection is a first example how the knowledge obtained in the study of the electronic decay of inner valence ionized clusters yields valuable insight into the physics of molecular Auger decay. Auger decay in *atoms* produces double vacancies in the *atomic* valence shells. Likewise Auger decay in molecules produces double vacancies in the valence molecular orbitals. The following discussion uses $2p$ ionized silicon atoms and $2p$ ionized SiF $_4$ as an example to discuss the general concepts. The Auger spectrum of $2p$ ionized silicon atoms exhibits a three-region structure. Each region is characterized by the dicationic final states p^{-2} , $p^{-1}s^{-1}$ and s^{-2} in the atomic valence shell.

Core holes in singly ionized molecules or solids are highly localized. Therefore it is frequently assumed that the Auger decay rate matrix elements are dominated by intra-atomic terms. For this reason it has been thought that the contribution of the molecular orbitals to the molecular Auger decay may be approximated by that of the atomic orbitals of the atom carrying the initial vacancy. In this picture, the chemical bond is seen as small modulation. This is called the *self-imaging picture* of molecular Auger decay⁹ (and references therein) and the Auger spectrum of a molecule exhibits the structure of atomic Auger decay, described above. A prominent example is the $1s$ Auger spectrum of fluorine which exhibits similar appearance in different materials. This picture of Auger decay in molecules is only valid if the molecular orbitals are very similar to the atomic orbitals of the initially ionized atom.

If this condition is not fulfilled, the situation changes dramatically⁹⁻¹². A good example for this situation is silicon tetrafluoride. The bonds in SiF $_4$ are highly polarized towards the fluorine atoms, causing a significant depletion of valence electrons on the silicon atom. The Auger spectrum of Si $2p$ ionized SiF $_4$ exhibits eight, instead of three, distinct regions because of the eight possibilities to produce two holes in the valence molecular orbitals: 1. F $_1 p^{-1}$ F $_2 p^{-1}$, 2. F p^{-2} (triplet), 3. F p^{-2} (singlet), 4. F $_1 p^{-1}$ F $_2 s^{-1}$, 5. F $p^{-1}s^{-1}$ (triplet), 6. F $p^{-1}s^{-1}$ (sin-

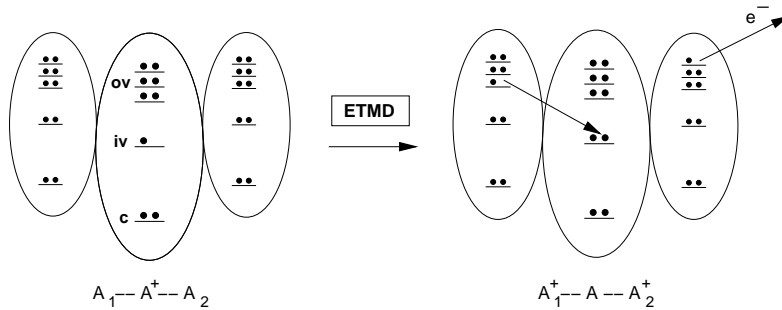


FIG. 5: Principle of three-monomer electron transfer mediated decay. A valence electron of A_1 drops into the hole on A and the excess energy is transferred to a valence electron of A_2 . A , A_1 , A_2 : atoms, ov : outer valence orbital, iv : inner valence orbital, c : core orbital. The inner valence IP of A is higher than the double ionization threshold for ionization from A_1 and A_2 .

glet), 7. $F_1 s^{-1} F_2 s^{-1}$, 8. $F s^{-2}$ in increasing energetical order. Orbitals associated with the silicon atom play practically no role. Here, F_1 and F_2 refer to different fluorine atoms. As can be seen, the Auger decay of the $Si 2p$ core hole populates only states with two valence holes essentially on the fluorine atoms. This phenomenon is termed the *foreign-imaging picture* of molecular Auger decay^{9,10}.

The mechanism responsible for this drastic redistribution of charge has been an open question. The arguments to be used in the case of foreign imaging parallel those given in subsection V E for the xenon fluorides. Therefore we give here only an abbreviated analysis. In the light of the preceding subsections, the foreign imaging phenomenon can be explained by resorting to interatomic electronic decay processes. The fact that the initial core hole is a $Si 2p$ hole and that the vast majority of final state holes are situated on one or two neighboring fluorine atoms¹⁰ suggests that ETMD is the dominant decay process because ETMD is the only process that produces final state holes on neighboring atoms exclusively. As no partial decay widths have been computed for ETMD in SiF_4 the impact of the transition matrix elements in (16) are unknown.

A reason for the intra-atomic rate to drop below the ICD, two- and three-atomic ETMD rates is the ionic bonding in SiF_4 because the outer valence electron density is considerably reduced on the central silicon atom. This extreme depletion of valence electron density on silicon causes the dominance of ETMD. To prove this one has to calculate the partial decay widths of the various decay processes in SiF_4 which has not been done yet.

We would like to study a new example for the surprising impact of the ideas presented so far. To this end, we examine the decay of $Xe 4d$ vacancies in XeF_n where interatomic processes lead to an increase in line width. To pursue this issue we need to introduce a couple of computational techniques in the ensuing sections III and IV. Readers not interested in much details should proceed with section V.

III. COMPUTATIONAL METHODS

A. Algebraic Diagrammatic Construction

Greens function methods are well-suited to calculate various properties of molecules. The pole positions of the particle propagator and the pole positions of the two-particle propagator yield the vertical IPs and DIPs of a molecule, respectively^{33–36}. The residuum or pole strength of the poles of the propagators is a measure of the one-particle or two-particle character of a specific singly or doubly ionized state, respectively, i.e. it is a measure how well the physical state is described by the $1h$ - or $2h$ -configurations that derive from the Hartree-Fock ground state.

Algebraic diagrammatic construction (ADC) is an approximation scheme for the particle and two-particle propagator using Feynman diagrams^{37–40}. The n -th order ADC scheme, $ADC(n)$ for short, contains infinite summations of those classes of diagrams which derive from the first n orders of the Feynman-Dyson perturbation series. The problem of finding their pole positions and pole strengths is formulated in terms of the solution of a Hermitian matrix eigenvalue problem. The eigenvalue problem is solved by a block-variant of the Lanczos algorithm which selectively computes the eigenvalues of a matrix^{41–43}. The Lanczos algorithm converges rapidly for the lowest and the highest eigenvalues. Unfortunately, the lowest IPs correspond to eigenvalues amidst the spectrum because the electron affinities of the molecule which are also given by poles of the one-particle Green's function are lower in energy.

The one-particle ADC scheme used to calculate the IPs in this work employs the Dyson equation which sums many diagram classes in addition to the summation carried out by the ADC scheme. Using the Dyson equation implies the combined calculation of the IPs and the electron affinities. The latter are also given by pole positions of the particle propagator. This enlarges the aforementioned eigenvalue problem extremely. Therefore an approximation to the affinity block in the Dyson equation

is made by replacing it with the much smaller result of a few block Lanczos iterations performed on this block⁴³.

Ionization from the Xe $4d$ orbitals of the xenon fluorides is a core-level ionization, with IPs widely above the double ionization threshold. Therefore, not only $2h1p$ -configurations but also $3h2p$ -configurations are expected to have a considerable impact for the description of these IPs^{44,45}. The ADC(3) scheme does not contain $3h2p$ -configurations explicitly, but the next order scheme, ADC(4), does. Hence one expects that the ADC(4) scheme gives an appreciable improvement of the core-level IPs of xenon and its fluorides.

The inclusion of $3h2p$ -configurations enlarges the configuration space considerably. The available computer resources are not sufficient to calculate a molecule like XeF₆ in an acceptable time. Therefore, the existing ADC(4) programs^{44–46} contain the core-valence separation approximation for core-level ionization which reduces the size of the configuration space and consequently does not calculate the ionization potentials of the valence regime. In particular, they do not include those $2h1p$ -configurations that are needed to describe core-hole decay. For these reasons, the ADC(4) programs are useless for the calculations needed here. Hence all ionization spectra were calculated using the ADC(3) scheme.

There is no Dyson equation for the two-particle Greens function^{47–49}. Therefore the two-particle ADC evaluates the two-particle propagator directly. The program⁴⁶ used to calculate double ionization potentials implements the two-particle ADC(2) scheme³⁹.

B. Two-Hole Population Analysis

The two-hole population analysis is a means to reveal the localization of the two holes which result from double ionization^{8,23}. It is used together with the ADC(2) program and is carried out by taking the contribution of the $2h$ -configurations to the total $2h$ -pole strength. To this end, a dicationic final state in the ADC(2) scheme is expanded in terms of $2h$ -configurations

$$|\Psi_n^{N-2}\rangle = \sum_{ij} (\vec{X}_n)_{ij} \underbrace{\hat{c}_i \hat{c}_j}_{2h\text{-config}} |\Phi_0\rangle + \dots, \quad (1)$$

where \vec{X}_n is the $2h$ -part of the ADC eigenvector of the n -th dicationic state. ij denotes a *single* $2h$ -configuration and \hat{c}_i , \hat{c}_j are annihilation operators acting on the Hartree-Fock ground state $|\Phi_0\rangle$. The correlated ground state of the system is approximated by the Hartree-Fock ground state^{50–52}. The two-hole population analysis^{8,23} examines only the $2h$ -components because in most cases the two-particle ADC(2) matrices cannot be diagonalized fully. The $3h1p$ -components of the eigenvectors are therefore typically not available.

The two-hole configurations can be either singlet or triplet states. There is no coupling between the two sets

of configurations with different spin. A spin adapted $2h$ -configuration in molecular orbital basis $|ij^{(s,t)}\rangle$ can be expanded^{8,23} in $2h$ -configurations $|pq^{(s,t)}\rangle$ deriving from the atomic orbital basis

$$|ij^{(s,t)}\rangle = \sum_{pq} U_{pq,ij}^{(s,t)} |pq^{(s,t)}\rangle. \quad (2)$$

The superscripts s and t denote singlet or triplet spin multiplicity, respectively, and ij and pq are hole indices in the molecular and atomic basis.

For a specific state $|\Psi_n^{N-2}\rangle$ the spin multiplicity is fixed. As the equations in this section possess an invariant form with respect to spin, the spin indices can be dropped. With the equations (1) and (2) one can express the n -th dicationic state in terms of the $2h$ -functions in atomic orbital basis

$$\begin{aligned} |\Psi_n^{N-2}\rangle &= \sum_{ij} (\vec{X}_n)_{ij} |ij\rangle + \dots \\ &= \sum_{pq} \sum_{ij} U_{pq,ij} (\vec{X}_n)_{ij} |pq\rangle + \dots \end{aligned} \quad (3)$$

This gives new expansion coefficients $\vec{Y}_n := \mathbf{U} \vec{X}_n$. Using this new vector to transform the total $2h$ -weight (ADC pole strength) gives^{8,23}

$$\vec{X}_n^\dagger \vec{X}_n = \vec{Y}_n^\dagger \mathbf{O} \vec{Y}_n = \sum_{pq} \underbrace{\left[Y_{pq,n} \sum_{rs} O_{pq,rs} Y_{rs,n} \right]}_{Q_{pq,n}} \quad (4)$$

where $O_{pq,rs} = \langle pq | rs \rangle$ denotes the overlap matrix of the $2h$ -configurations in atomic orbital basis. The orthonormality condition for the molecular orbitals thus reads $\mathbf{U}^\dagger \mathbf{O} \mathbf{U} = \mathbf{1}$. The $Q_{pq,n}$ form the $2h$ -population matrix. Choosing suitable sets of atomic basis functions A , B , one obtains population numbers^{8,23}

$$Q_{AB,n} = \sum_{\substack{p \in A \\ q \in B}} Q_{pq,n}. \quad (5)$$

Frequently, as is done in this work, A and B represent the atomic basis functions of individual atoms within a molecule. This provides a clear picture of the localization properties of the two holes.

As the contribution to the $2h$ -pole strength is used in this population analysis, the sum of the contributions $\sum_{pq} Q_{pq,n}$ to the n -th dicationic state yields the $2h$ -pole strength of this state. In this work, all population numbers of the n -th state are normalized, so summing them yields 1. Then, the numbers $Q_{AB,n}$ represent the fraction of the two holes to be located on the atoms A and B .

C. Wigner-Weisskopf Theory

Wigner-Weisskopf theory^{24,25} applies time-dependent perturbation theory to describe the decay of a resonance.

The theory yields an approximation to the decay width and was applied in Refs. 17,19 to inner-valence-ionized clusters to study their electronic decay. There, single Hartree-Fock determinants were employed to describe initial and final states which is not suitable here.

Let the initial state $|\Psi_I\rangle$ be a singly ionized resonance state and the final states $|\Psi_F\rangle$ are the n -th doubly ionized state together with the free electron of momentum \vec{k} resulting from the decay. The decay width is given by^{24,25}

$$\Gamma = 2\pi \sum_{F \neq I} |\langle \Psi_F | \hat{H} | \Psi_I \rangle|^2 \delta(E_F - E_I). \quad (6)$$

This equation contains three types of matrix elements: $\langle \Psi_F | \hat{H} | \Psi_I \rangle$ transition matrix element, $E_I := \langle \Psi_I | \hat{H} | \Psi_I \rangle$ initial state energy and $E_F := \langle \Psi_F | \hat{H} | \Psi_F \rangle$ final state energy. The δ -function in equation (6) assures that the contribution to the total decay width of only those accessible final states is summed that conserve energy in the decay.

The partial decay widths of the various electronic decay processes, intra-atomic electronic decay, ICD, two- and three-monomer ETMD which are reviewed in section II can be described by expressions of the type (6) in Wigner-Weisskopf theory^{24,25}. All four decay processes have in common that they produce two final state holes. One sums over all energetically accessible dicationic final states which are denoted below with the single index n , to obtain the total decay width

$$\Gamma_{\text{ch}} = \sum_n \Gamma_n = \Gamma_{\text{One-site}} + \Gamma_{\text{Two-site}}. \quad (7)$$

of the initial core hole ‘‘ch’’. There are two sorts of overall partial decay widths. The electronic decays which produce two holes localized on one atom, the *one-site states*, and those which produce two holes localized on two atoms, the so-called *two-site states*. The one-site final states arise from intra-atomic electronic decay and two-monomer ETMD, as shown in figures 2, 4

$$\Gamma_{\text{One-site}} = \Gamma_{\text{Intra-atomic}} + \Gamma_{\text{ETMD},2}. \quad (8)$$

ICD and three-monomer ETMD produce two-site final states, as shown in figures 3, 5

$$\Gamma_{\text{Two-site}} = \Gamma_{\text{ICD}} + \Gamma_{\text{ETMD},3}. \quad (9)$$

Of course, each of the above partial widths can be viewed as a sum over the accessible final states. For instance, $\Gamma_{\text{ICD}} = \sum_n \Gamma_{n, \text{ICD}}$.

D. On the Lifetimes of Decaying States

The calculation of lifetimes $\tau = 1/\Gamma$ of decaying electronic states with a decay width Γ is, in general, much more complicated than the calculation of the energy

of stationary states²⁸. In addition, the decay electron, i.e. the electron emitted as the result of the decay of the core hole levels, is inappropriately represented in Gaussian basis sets typically used in quantum chemistry calculations²⁸. Nevertheless, Wigner-Weisskopf theory^{24,25} and the population numbers discussed above can be used to analyze the decay at least qualitatively.

To this end, we return to the decay width in (6) and observe that a final state of the decay can be written as $|\Psi_n^{\vec{k}}\rangle$ where n specifies the dicationic state and \vec{k} the momentum of the emitted electron. For simplicity we employ the sudden approximation (Ref. 53 and references therein) and express $|\Psi_n^{\vec{k}}\rangle$ by the antisymmetrized product $\hat{c}_k^\dagger |\Psi_n\rangle$. We now expand the dicationic state in terms of dicationic electronic configurations using, for instance, the expansion (1) and obtain

$$\langle \Psi_n^{\vec{k}} | \hat{H} | \Psi_I \rangle = \sum_{ij} (\vec{X}_n^\dagger)_{ij} \langle \Phi_{ij}^{\vec{k}} | \hat{H} | \Psi_I \rangle + \dots \quad (10)$$

for the transition matrix elements in (6). Here, the final state configurations are given by $|\Phi_{ij}^{\vec{k}}\rangle = \hat{c}_k^\dagger \hat{c}_i \hat{c}_j |\Phi_0\rangle$. If we further assume that the initial state can be approximated by a single determinant $|\Psi_I\rangle = \hat{c}_l |\Phi_0\rangle$ where l indicates a core orbital index, and that core orbitals do not contribute to the $(\vec{X}_n^\dagger)_{ij}$ of the final state which is a good approximation, then the terms indicated in (10) as ‘‘...’’ vanish exactly due to the Slater-Condon rules³³.

To proceed we make use of (2) which enables us to express the dicationic electronic configurations in terms of atomic $2h$ -indices pq . The configurations $|\Phi_{ij}^{\vec{k}}\rangle$ appearing in (10) form an orthonormalized set of functions and by using the relation

$$|\Phi_{ij}^{\vec{k}}\rangle = \sum_{pq,rs} (\mathbf{O}^{\frac{1}{2}})_{pq,rs} U_{rs,ij} |\Phi_{pq}^{\vec{k}}\rangle \quad (11)$$

we have introduced an orthonormalized set of configurations $|\Phi_{pq}^{\vec{k}}\rangle$ in terms of atomic orbitals in (2). Notice that the atomic configurations in (2) are not orthonormalized. Inserting (11) into (10) leads to

$$\langle \Psi_n^{\vec{k}} | \hat{H} | \Psi_I \rangle = \sum_{pq} Y'_{pq,n} \langle \Phi_{pq}^{\vec{k}} | \hat{H} | \Psi_I \rangle \quad (12)$$

where $\vec{Y}'_n := \mathbf{O}^{\frac{1}{2}} \mathbf{U} \vec{X}_n$. This equation relates the transition matrix element to a superposition of atomic-like quantities.

We now insert the transition matrix element (12) into the basic equation (6) for the decay width, integrate over the momentum \vec{k} of the emitted electron and neglect interference terms (cross terms). The result reads

$$\begin{aligned} \Gamma &= \sum_n \Gamma_n \\ \Gamma_n &= \sum_{pq} |T_{pq}|^2 |Y'_{pq,n}|^2. \end{aligned} \quad (13)$$

The width associated with the final dicationic state $|\Psi_n\rangle$ specified by n is expressed as a sum over $2h$ -atomic indices. Each contributing term consists of a state specific factor $|Y'_{pq,n}|^2$ which we have calculated above. The other factor

$$|T_{pq}|^2 = 2\pi \sum_{\vec{k}} |\langle \Phi_{pq}^{\vec{k}} | \hat{H} | \Psi_I \rangle|^2 \delta(E_F - E_I) \quad (14)$$

depends on the dicationic state $|\Psi_n\rangle$ only via the $\delta(E_F - E_I)$ function. Since we consider the decay of a core level implying that the energy of the emitted electron is high, this dependence is weak and can be neglected to a good approximation.

The state specific quantities $|Y'_{pq,n}|^2$ are closely related to the occupation numbers discussed above in section III B. In principle, they could be used as an alternative definition of occupation numbers (in spirit of Löwdin's population analysis³³). In particular, if the atomic basis functions are well localized, each on its atom, we may put $|Y'_{pq,n}|^2 = Q_{pq,n}$ and obtain

$$\Gamma_n = \sum_{pq} |T_{pq}|^2 Q_{pq,n} . \quad (15)$$

For a given molecule the quantities $|T_{pq}|^2$ are universal and the only information which is state specific is in the occupation numbers $Q_{pq,n}$. We are able to compute the occupation numbers of the molecules studied in this work and hence (15) is already a useful tool of analysis.

The number of distinct atomic pairs (pq) is, unfortunately, rather large. We notice, however, that many elements $|T_{pq}|^2$ are of similar magnitude, e.g., if p denotes a p -type atomic orbital on atom A and q a p -type atomic orbital on atom B , and group together in (15) the corresponding contributions: $\Gamma_n = |T_{AB}|^2 \sum_{\substack{p \in A \\ q \in B}} Q_{pq,n} + \dots$

Since $|T_{pq}|^2$ grouped together are not identical, the average quantity $|T_{AB}|^2$ will slightly depend on the dicationic state index n . Computing $\Gamma = \sum_n \Gamma_n$ amounts to averaging over the slightly varying $|T_{AB}|^2$ and thus leads to a more stable result. We may now classify the atomic pairs (pq) by their localization characteristics. Let us denote with A the atom on which the initial core hole is localized. Then, if p and q denote atomic orbitals on A , obviously $|T_{pq}|^2$ corresponds to intra-atomic electronic decay. Analogously, if p belongs to atom A and q to atom B , we are dealing with ICD, and if neither p nor q belong to A , $|T_{pq}|^2$ describes two- or three-monomer ETMD depending on whether p and q belong to the same atom B or not. Thus, the *minimal* dissection of Γ into its various contributions in the spirit of the above discussion

reads

$$\begin{aligned} \Gamma = & |T_{\text{intra-atomic}}|^2 \sum_n \sum_{p,q \in A} Q_{pq,n} \\ & + |T_{\text{ICD}}|^2 \sum_n \sum_{\substack{p \in A \\ q \in B}} Q_{pq,n} \\ & + |T_{\text{ETMD},2}|^2 \sum_n \sum_{p,q \in B} Q_{pq,n} \\ & + |T_{\text{ETMD},3}|^2 \sum_n \sum_{\substack{p \in B \\ q \in C}} Q_{pq,n} . \end{aligned} \quad (16)$$

If necessary, further dissections of Γ into more detailed contributions are readily done. For instance, grouping together separately the contributions of p and q both being atomic orbitals of s -type, both of p -type, or one of s - and one of p -type, etc. A distinction between the decay into singlet and triplet final dicationic states is also possible. Finally, we mention that the individual transition strengths $|T_{\text{ICD}}|^2$, etc., may be similar in a series of related molecules.

IV. COMPUTATIONAL DETAILS

The ground state geometries of F_2 , XeF_2 , XeF_4 and XeF_6 are taken from literature. The distance of the fluorine atoms in the fluorine molecule is $r(\text{F-F}) = 1.42 \text{ \AA}$ ⁵⁴. Xenon(II)-fluoride also is a linear molecule of $D_{\infty h}$ symmetry with a Xe-F distance of 1.977 \AA ⁵⁴. Xenon(IV)-fluoride is square-planar (D_{4h}), the Xe-F distance is 1.94 \AA . See chapter 12 in Ref. 54 for further chemical and physical properties of the xenon fluorides. The atomic distances are given for all molecules in the gas phase.

The ground state geometry of xenon(VI)-fluoride *in gas phase* is a distorted octahedron^{21,55}, it can be described in C_{3v} symmetry. Nevertheless, some of our computations were performed in O_h symmetry due to computer hardware limitations. The notation of figure 1a in Ref. 55 is used here. Our calculations on XeF_6 in C_{3v} symmetry use the bond lengths $r(\text{Xe-F1}) = 1.856 \text{ \AA}$ and $r(\text{Xe-F4}) = 1.972 \text{ \AA}$ and bond angles $\alpha = 80.8^\circ$ and $\beta = 112.8^\circ$ taken from tables 2,3 of Ref. 55. These values have been determined using MP2 and an all-electron basis with f -functions. Our computations on XeF_6 in O_h symmetry were performed at the bond length $r(\text{Xe-F}) = 1.952 \text{ \AA}$ which is taken from table 1 of Ref. 55.

The ADC programs, used for the calculation of single and double ionization potentials, introduced in section III A rely on the molecular orbitals of a Hartree-Fock calculation which are obtained using the GAMESS-UK⁵⁶ program package. The employed software uses no symmetry for the xenon atom. D_{2h} symmetry is used for F_2 , XeF_2 and XeF_4 . The calculation of the single ionization potentials of XeF_6 in the ground state geometry of C_{3v} symmetry is performed in C_s symmetry.

The double ionization spectrum of XeF_6 is calculated using a ground state geometry of O_h symmetry, instead

of C_{3v} symmetry, to make the calculation feasible with the available computer resources. The employed software uses D_{2h} symmetry to calculate the DIPs of XeF_6 in the ground state geometry of O_h symmetry. To investigate the effect of the different symmetries of the ground state of XeF_6 , the orbital energies are compared. The overall positions of the xenon-like orbitals are in good agreement in both symmetries but the split of the fluorine-like orbitals is enlarged due to the increased interaction in C_{3v} symmetry.

The xenon and the fluorine atoms are represented by the DZVP (DFT orbital)^{57,58} basis set. The quality of the basis sets can be estimated from table I by comparing the Hartree-Fock orbital energies of xenon, obtained by solving the Hartree-Fock equations numerically, i.e. without the help of an initially given fixed basis set⁵⁹, with those obtained using the DZVP (DFT orbital)^{57,58} basis set. The shift of the orbitals, due to the approximation introduced by the finite basis set, are $\Delta\varepsilon_{\text{BS}} := \varepsilon_{\text{HF, numeric}} - \varepsilon_{\text{HF, DZVP}}$. The shift is ≈ 0.1334 eV for the Xe $4d$ orbitals and even less for the valence orbitals because basis sets are usually optimized with respect to the latter orbitals. This shift is neglected in the following because other errors are larger.

There are three main relativistic effects one has to take into account when examining heavy atoms like xenon^{60,61}:

1. the relativistic radial contraction and energetic stabilization of the s and p shells,
2. the spin-orbit splitting,
3. the relativistic radial expansion and the energetic destabilization of the (outer) d and f shells.

Effects (1) and (3) are termed scalar relativistic effects⁵⁵.

As the theory of subsection III A for the calculation of IPs is strictly non-relativistic, one has to take into account relativistic effects by a ‘‘rule of thumb’’. This is done by performing Hartree-Fock and Dirac-Fock calculations, the relativistic counterpart to Hartree-Fock^{60,61}, for the xenon atom. Due to the spherical symmetry of atoms, the equations can be solved numerically^{59,62,63}, i.e. without fixed basis sets, to arbitrary precision. This gives exact sets of relativistic and non-relativistic orbitals in the mean field approximation.

In table I, the orbitals determined in this way are listed together with Hartree-Fock orbitals obtained by a calculation employing the DZVP (DFT Orbital)^{57,58} basis set. By comparing the orbital energies of the two numerical solutions of the Hartree-Fock and Dirac-Fock equations, one can determine the size of relativistic effects and correct for them in non-relativistic computations of the IPs of the xenon fluorides.

To carry out this comparison, one has to note that the total angular momentum j is the combination of the orbital angular momentum l and the electron spin: $j = l \pm \frac{1}{2}$. A Dirac-Fock calculation yields two orbitals⁶⁰, one

for $j_+ = l + \frac{1}{2}$ and one for $j_- = l - \frac{1}{2}$, for one Hartree-Fock orbital with $l \geq 1$. The j_- orbital has a lower orbital energy than the j_+ orbital.

To compare Dirac-Fock with Hartree-Fock orbital energies one has to calculate a weighted mean of the two Dirac-Fock orbital energies⁶⁰, which effectively removes spin-orbit splitting. This weighted mean reads

$$\bar{\varepsilon}_{\text{DF}} = \frac{(2j_+ + 1)\varepsilon_{\text{DF},+} + (2j_- + 1)\varepsilon_{\text{DF},-}}{2j_+ + 1 + 2j_- + 1}. \quad (17)$$

The scalar relativistic shift of the non-relativistic orbitals is $\Delta\varepsilon := \bar{\varepsilon}_{\text{DF}} - \varepsilon_{\text{HF}}$. The shifts are 3.077 eV for the Xe $4d$, -1.789 eV for the Xe $5s$ and -0.00283 eV for the Xe $5p$ orbitals. The sign of the shift is predicted by the rules (1) and (3) given above because the energetic stabilization of s and p orbitals leads to a lowering of the Xe $5s$ and Xe $5p$ orbital energies and thus $\Delta\varepsilon < 0$. Similarly, $\Delta\varepsilon > 0$ holds for the shift of the Xe $4d$ orbital energies due to the energetic destabilization of the (outer) d orbitals.

Koopmans’ theorem^{33,64} states that the IPs of an atom or a molecule are approximately given by the negative of the orbital energies $IP \approx -\varepsilon_{\text{HF}}$. As the relativistic shift $\Delta\varepsilon$ represents a relativistic correction to the Hartree-Fock orbital energies $\varepsilon_{\text{HF,corr}} = \varepsilon_{\text{HF}} + \Delta\varepsilon$, the IPs are corrected as follows $IP_{\text{corr}} = IP_{\text{HF}} - \Delta\varepsilon$.

The above shifts of the orbital energies of the xenon atom are used to correct the Xe $4d$ orbitals for the scalar relativistic effect by adding $-\Delta\varepsilon$ to the Xe $4d$ IP of the non-relativistic calculations. This procedure is justified by the observation that the Xe $4d$ orbitals are highly localized and are very similar to atomic Xe $4d$ orbitals. The Xe $4d$ IPs calculated employing the ADC(3) scheme take electron correlation into account. Therefore contributions of all orbitals mix into the description of the Xe $4d$ ionized states. As the Xe $4d$ ionized states are predominantly described by the Xe $4d$ orbitals the relativistic correction is applicable in this case as well.

The spin-orbit split in the xenon atom amounts to 2.111 eV for the $4d$ orbitals and 1.436 eV for $5p$ orbitals (table I). The spin-orbit split in the xenon atom is possibly only a good approximation²¹ for the Xe $4d$ orbitals in the xenon fluorides because the Xe $5p$ orbitals suffer from a significant modification by the molecular bond to the fluorine atoms. The experimental value for the spin-orbit split of the $4d$ orbitals in the xenon atom is 1.984 ± 0.014 eV (table III). The theoretically and experimentally determined values are in satisfactory agreement. A good agreement is not expected because the Dirac-Fock equations are a mean field approximation⁶⁰ and do not take electron correlation into account. Spin-orbit splitting is not accounted for in the non-relativistic theory used throughout and is not considered any further in the ensuing sections.

The double ionization spectra cannot be corrected for the relativistic effects as easily as the single ionization spectra because usually two orbitals with different orbital angular momenta are involved. Our computed double ionization spectra are only accurate up to the Xe $4d$ ion-

HF orbital	$\epsilon_{\text{HF, DZVP}}$	$\epsilon_{\text{HF, numeric}}$	DF orbital	ϵ_{DF}	$\bar{\epsilon}_{\text{DF}}$
4d	-2.78280	-2.77788	4d _{3/2}	-2.71133	-2.66479
			4d _{5/2}	-2.63376	
5s	-0.946253	-0.944414	5s	-1.01014	-1.01014
5p	-0.457894	-0.457290	5p _{1/2}	-0.492572	-0.457394
			5p _{3/2}	-0.439805	

TABLE I: Hartree-Fock (HF) and Dirac-Fock (DF) orbital energies of xenon. Hartree-Fock orbitals are given for the DZVP (DFT orbital)^{57,58} basis set and for the numeric solution. The Dirac-Fock orbitals were obtained numerically. All data are given in Hartree.

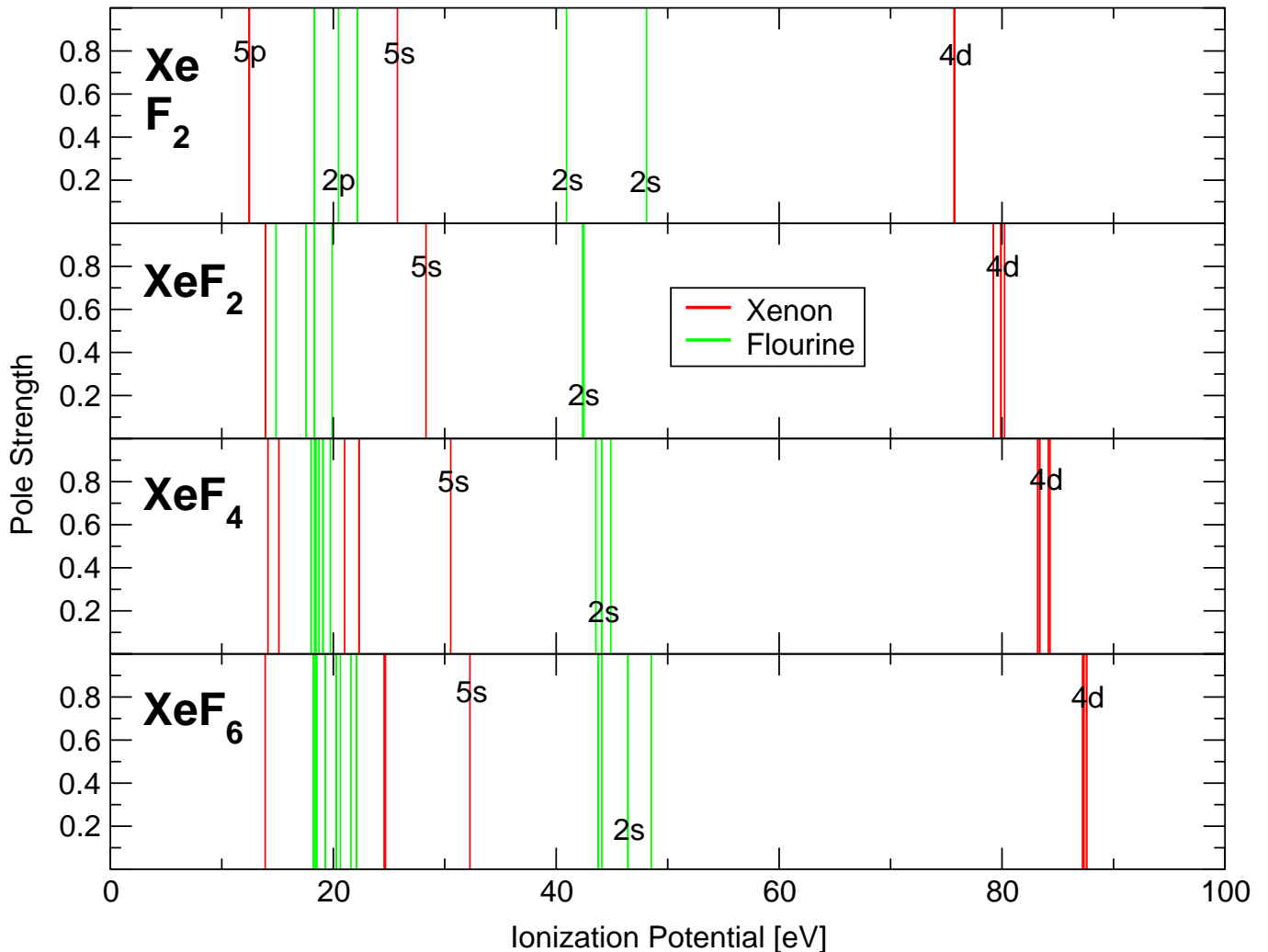


FIG. 6: (Color) Single ionization spectra of Xe, F₂, XeF₂, XeF₄ and XeF₆ calculated on Hartree-Fock level (Koopmans' theorem). The assignment of the lines to atomic orbitals of xenon or fluorine origin in XeF_n is not strict in the valence region due to the molecular bond.

ization energy where only the Xe 5p and Xe 5s orbitals are involved and the main relativistic error of the DIPs is caused by the neglect of the relativistic shift of the Xe 5s orbitals. The amount of spin-orbit coupling cannot be estimated satisfactorily for the double ionization spectra.

V. RESULTS AND DISCUSSION

A. Single Ionization Spectra

1. Mean-Field Model

Single ionization spectra of the xenon fluorides can be obtained with the help of Koopmans' theorem^{33,64} in the

Compound	Atoms	Nuclear Charge	Mulliken Population	Löwdin Population
XeF ₂	Xe	54	52.92	52.95
	2 F	9	9.54	9.53
XeF ₄	Xe	54	52.13	52.12
	4 F	9	9.47	9.47
XeF ₆	Xe	54	51.71	51.51
	3 F	9	9.49	9.51
	3 F	9	9.27	9.33

TABLE II: Mulliken and Löwdin population analyses of XeF₂, XeF₄ and XeF₆.

Hartree-Fock approximation. In this mean field model the correlation between the electrons is neglected resulting in very simple spectra (figure 6) which can give a hint for the interpretation of the more complex spectra that include electron correlation (figure 7). The assignment of the lines in figure 6 to atomic orbitals of xenon or fluorine is not strict in the valence region due to the molecular bond. In the lower lying molecular orbitals, this assignment is well-defined. As spin-orbit coupling is neglected, *artificial* degeneracies are introduced in the spectra of figure 6. The effect of the ligand field caused by the fluorine atoms is of course included.

The effect of adding fluorine atoms to xenon is studied by Mulliken and Löwdin population analyses^{33,65} in table II. We remind that such population analysis may exhibit some basis set dependence³³ but the consistency between the two sets of results indicates reliability. One sees immediately that charge is withdrawn from the xenon atom to the fluorine atoms: XeF₂: 1.1, XeF₄: 1.9, XeF₆: 2.3 electron charges. Due to the C_{3v} symmetry of the ground state geometry of XeF₆, there are two kinds of fluorine atoms with different distances to the central xenon atom. These geometric differences are reflected in table II in that these fluorine atoms in XeF₆ which are further away from the xenon atom acquire less charge.

At first sight one may assume that the computed change in charge density involves only the valence electrons and has little effect on the inner molecular orbitals of the xenon fluorides. In the hydrogen atom, the wave functions of the higher lying shells, which are unoccupied in the ground state, have a considerable amplitude in the spatial regions of the lower lying shells of the same angular momentum²⁴. As this argument also holds in the case of the xenon fluorides, a reduction of valence electron density on the xenon atom leads to a less efficient screening of its nuclear charge and consequently to a lowering in energy of the energetically low lying molecular orbitals with a dominant contribution on the xenon atom.

Conversely, the increase of valence electron density on the fluorine atoms leads to a more efficient screening of their nuclear charge and consequently raises the energy of the lower lying molecular orbitals with a dominant con-

tribution on fluorine atoms. The charge withdrawn from the xenon atom is shared among several fluorine atoms. The net increase of charge density on each fluorine atom is ≈ 0.5 electron charges. This value is, of course, much smaller than the loss of charge density on the xenon atom and hence the impact on the inner molecular orbitals of fluorine character is expected to be much smaller than for xenon. It is most dramatic in XeF₂ where each fluorine atom acquires the largest fraction of charge. The screening of the nuclear charge is largest in XeF₂ and decreases in XeF₄ and XeF₆.

The effects of this model can be seen in figure 6. The positions of the Xe 5*s* and Xe 4*d* lines shift to higher binding energies with an increasing number of fluorine atoms. The energy differences between the corresponding lines of XeF₂, XeF₄ and of XeF₄, XeF₆ are nearly equally large. The F 2*p* and F 2*s* lines also shift slightly to higher binding energies with increasing number of fluorine atoms. This explanation for the shift of the fluorine lines is supported by a comparison with F₂. The mean of the F 2*p* lines in F₂ and the mean of the F 2*s* lines in F₂ are higher in energy than the mean values of the corresponding lines in XeF₂. The first IP is nearly constant for all xenon fluorides studied. Its value is ≈ 12.5 eV.

In the fluorine molecule, the two F 2*s* lines are split considerably due to the molecular bond. The split of the two F 2*s* lines in XeF₂ is tiny due to the large separation of the fluorine atoms. In XeF₄ and XeF₆, the fluorine atoms are closer and interact. This results in a larger split of the F 2*s* lines in comparison to the split in XeF₂.

The Xe 4*d* lines are quintuply degenerate in the single ionization spectrum of the xenon atom in figure 6. In XeF₂, the degeneracy is lifted by the ligand field of the fluorine atoms and three distinct lines become visible. The three lines reflect the spatial orientation of the 4*d* orbitals. There is a ligand field along the molecular axis. Perpendicular to the molecular axis there is no shift resulting in a total of three lines. In XeF₄ there is only one dimension left that is unaffected by the ligand field: the axis perpendicular to the molecular plane. The spectrum, figure 6, shows that there are four distinct Xe 4*d* lines in this case.

In XeF₆ the situation changes because the fluorine atoms are grouped around the xenon in such a way that XeF₆ is close to octahedral symmetry. This high symmetry leads to a split of the two 4*d* orbitals of XeF₆ in O_h symmetry of only 0.1568 eV compared to the much larger splits in XeF₂ and XeF₄. Lowering the symmetry to C_{3v} leads in XeF₆ to three distinct 4*d* orbital energies with a total split of 0.3682 eV.

2. Correlation Effects

Going beyond the Hartree-Fock description of the molecules by using ADC(3) leads to the IPs plotted in figure 7. Figure 6 helps to identify the one-particle origin of the states in figure 7. The Xe 4*d* lines are energetically

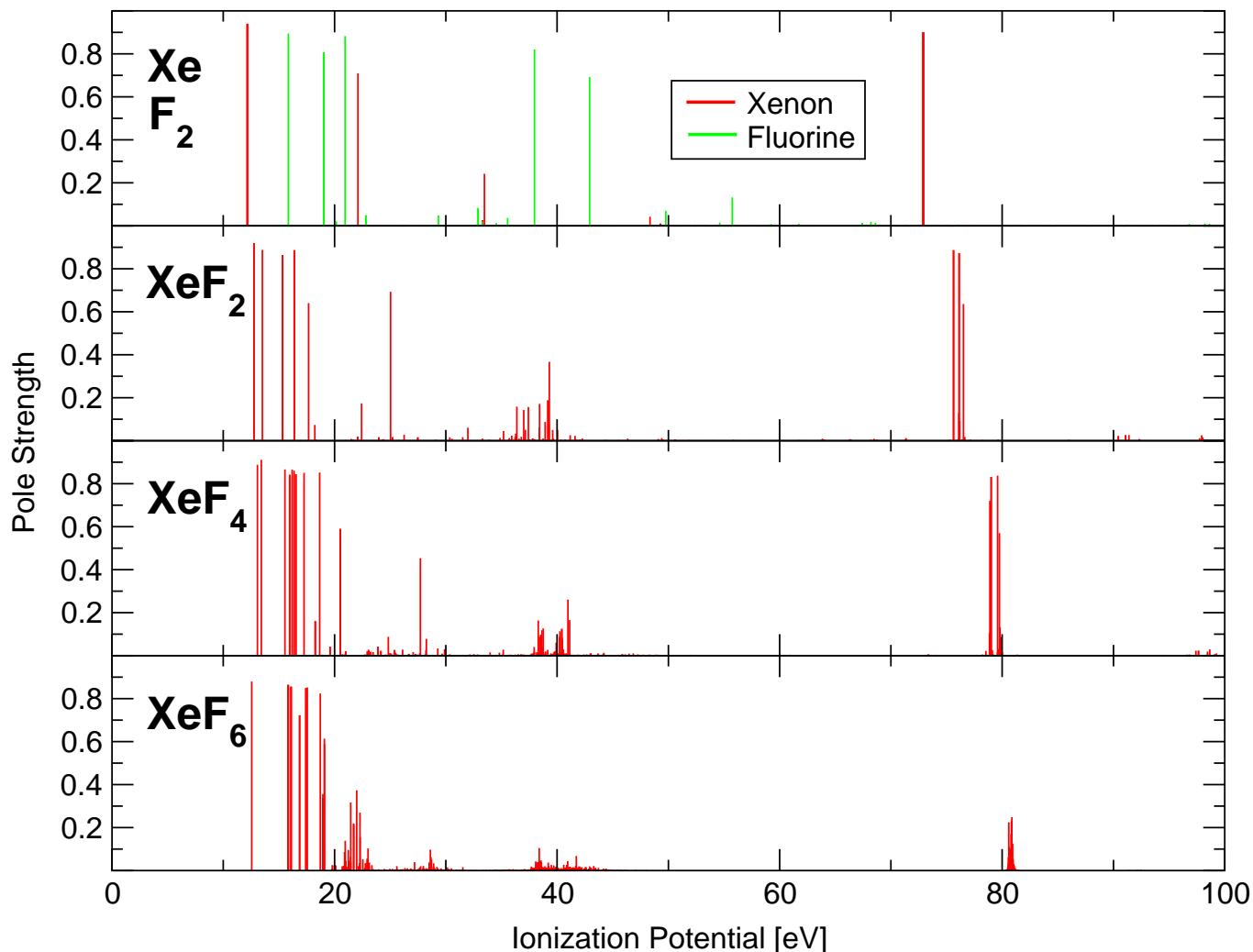


FIG. 7: (Color) Single ionization spectra of Xe, F₂, XeF₂, XeF₄ and XeF₆ calculated with the one-particle ADC(3) program (see text). The assignment of lines to atomic orbitals of xenon or fluorine origin is not done for the XeF_n molecules.

clearly separated from the outer and inner valence lines in all spectra. They are located between 72 eV and 82 eV. The F 2s derived lines show up between 35 eV and 45 eV. Correlation effects do not change the fact that the first IPs are approximately equal in all compounds.

There is an overall dramatic change of the spectra due to the inclusion of many-body effects which grows with increasing number of fluorine atoms. This is reflected in energy shifts and reduction of intensity in the outer valence part of the spectra, in the appearance of numerous satellite lines in the vicinity of 20 eV and above, and in particular in the eye catching breakdown of the molecular orbital picture of ionization seen in the inner valence region. The latter phenomenon is common in molecules⁶⁶; the intensity originally confined to a single orbital in figure 6 is spread over many cationic states (figure 7). The breakdown of the molecular orbital picture of ionization is caused by compact $2h1p$ -configurations which are close

in energy to a one-particle state and contribute considerably to the description of the state⁶⁶. The coupling of these configurations to one-particle states leads to a broad shape of lines which has been observed in the inner valence region of many molecules⁶⁶.

Due to the many-body description of a molecule by the ADC scheme, decay processes of electronic states of the ion which turn into resonances also become describable¹⁶. In particular, the final state of the electronic decay of a singly ionized molecule can be approximated in terms of $2h1p$ -configurations describing the emitted electron ($1p$) and the residual dication ($2h$)(see subsection III D). The shape of each decaying state can be identified as a thin bundle of lines which mimic a discretized Lorentzian curve¹⁶.

To unambiguously identify a decaying state the breakdown of the molecular orbital picture of ionization has to be separated clearly from the decaying states in a small

energy range where each decaying state mimics a discretized Lorentzian curve. Furthermore, there can be a mixing of both phenomena for a certain state, but it is hard to identify a decay curve for one-particle states that suffer from the breakdown phenomenon.

The inner valence region of the xenon fluorides comprises the Xe $5s$ and F $2s$ states. The F $2s$ states are subject to the breakdown phenomenon and may also decay by emitting an electron. The Xe $5s$ one-particle state suffers solely from breakdown. No decay is possible because its IP is below the double ionization threshold (see next subsection). Many $2h1p$ -configurations contribute to the Xe $5s$ one-particle state (see figure 7). As the Xe $5s$ line is close to the double ionization threshold, many $2h1p$ -configurations are close in energy to this state because the excited states are generally very dense in this energetic region.

The spectra exhibit a considerable increase of breakdown of the molecular orbital picture for the inner valence with an increasing number of fluorine atoms. Obviously, the number of possible configurations rises due to the addition of fluorine atoms. As xenon fluorides are very symmetric, these fluorine atoms are all equivalent (except for XeF₆ in C_{3v} symmetry) and the number of equivalent $2h1p$ -configurations with one hole on the xenon atom and one hole on a fluorine atom doubles between XeF₂ and XeF₄. In XeF₆ there are even more such configurations than there are in XeF₄ but they are no longer equivalent due to the C_{3v} symmetry of the XeF₆ ground state.

Another contribution to the increase of one-particle states involved in the breakdown phenomenon can be attributed to the decrease in symmetry: spherical symmetry (Xe), $D_{\infty h}$ (XeF₂), D_{4h} (XeF₄), C_{3v} (XeF₆). This decrease in symmetry leads to an increase in electronic configurations that can couple to the respective states.

The one-particle picture is a relatively good description for the Xe $4d$ lines. $2h1p$ -configurations close to the energy of the core $1h$ -configurations are spatially diffuse and thus couple only weakly to the core $1h$ -configurations. Therefore, the mixing of $2h1p$ -configurations with $1h$ -configurations is weak. The splits of the Xe $4d$ lines in the xenon fluorides are of comparable size to those in figure 6 and the individual lines can be identified easily in all molecules but XeF₆.

As in all xenon fluorides, the Xe $4d$ lines are above the double ionization threshold and the electronic decay of the Xe $4d$ -ionized xenon fluorides is possible (see next subsection). The Xe $4d$ lines in figure 7 show signs of decay by exhibiting signs of discretized Lorentzian curves. The shape of the discretization of the Lorentzian curve representing a decaying state in the spectra depends highly on the number of $2h1p$ -configurations in the energy range of the decay electron.

The decay electrons which result from the decay of a Xe $4d$ vacancy are highly energetic (up to ≈ 60 eV). Hence a satisfactory description in terms of Gaussian basis sets is not feasible. Therefore the Xe $4d$ IPs in

figure 7 correspond in our description essentially to one-particle states (a pole strength close to unity). Nevertheless, the number of states which originate from $2h1p$ -configurations around the Xe $4d$ IPs grows with the number of fluorine atoms. In XeF₆ one observes very densely lying states around 83 eV with a high contribution of $2h1p$ -configurations. The extreme change in the importance of $2h1p$ -configurations in XeF₆ compared to XeF₄, XeF₂ was investigated by us.

The six fluorine atoms in XeF₆ form a distorted octahedron around the xenon atom. Hence the basis of the fluorine atoms may help to improve the description of the decay electrons from Xe $4d$ -ionized XeF₆ considerably. To test this assumption, the ionization spectrum of XeF₂ was calculated with the DZVP (DFT orbital)^{57,58} basis set augmented by a few diffuse functions. The resulting spectrum did not change much compared to that of figure 7.

To test the effect of the basis functions on the fluorine atoms, we performed another calculation of the ionization spectrum of XeF₂ with fluorine basis functions attached to ghost centers arranged to yield an octahedron of fluorine basis functions surrounding the central xenon atom. The extra basis functions had a minor effect on the spectrum and did not account for the drastic effect observed in figure 7 for XeF₆. These investigations convinced us of the suitability of the DZVP (DFT orbital)^{57,58} basis set for our concerns but did not elucidate the reasons for the drastic change in figure 7. To this end, we calculated the ionization spectrum of XeF₆ using O_h symmetry. The resulting spectra showed a similar shape of the Xe $4d$ lines as that of Xe $4d$ lines in XeF₄ revealing the great importance of the decreased symmetry for the description of XeF₆ in our computations. The reduction in symmetry from O_h to C_{3v} enables a vastly enlarged amount of $2h1p$ -configurations to couple to the Xe $4d$ $1h$ -configuration. To some extent this is similar to an increased basis set, as a multitude of configurations are provided additionally for the description of the ionized states. For sure this improves the description of decay electrons with a low kinetic energy.

The charge transfer from the xenon atom to the fluorine atoms, discussed in subsection V A 1, leaves a positively charged central xenon atom. Therefore, it is not surprising that XeF₄ and XeF₆ possess positive electron affinities, i.e. (XeF₄)⁻ and (XeF₆)⁻ are stable anions. We have computed the respective electron affinities by ADC(3). The values obtained for XeF₄ (a doubly degenerate state) is 0.66 eV and there are electron affinities of XeF₆ at 1.30 eV, 1.31 eV, 1.81 eV. The figures are not very accurate because the basis set is not very well suited to describe the diffuse states of anions. In XeF₆ the fluorine atoms form a cloud of nearly octahedral symmetry of negative charge around the central positively charged xenon atom. This potential well is similar to potential well used in the model problem discussed in^{28,67,68}. There scattering a particle off a potential well is investigated.

Cmpd.	Line	IP_{exp}	IP_{ADC}	IP_{rel}	Γ_{exp}
Xe	1	69.525 (10)	72.90	69.82	0.207 (4)
	2	67.541 (9)			0.202 (4)
XeF ₂	1	72.568 (6)	76.52	73.44	0.248 (8)
	2	72.248 (6)	76.14	73.06	0.223 (10)
	3	70.601 (13)	75.63	72.55	0.264 (26)
	4	70.421 (9)			0.256 (27)
	5	70.179 (6)			0.214 (19)
XeF ₄	1	75.098 (6)	79.76	76.68	0.319 (8)
	2	74.729 (7)	79.60	76.52	0.255 (8)
	3	73.140 (10)	79.01	75.93	0.392 (10)
	4	72.816 (10)	78.89	75.81	0.210 (27)
	5	72.661 (5)			0.225 (26)
XeF ₆	1	77.462 (13)	80.86	77.78	0.32 (4)
	2	77.321 (11)	80.59	77.51	0.25 (3)
	3	75.53			0.33
	4	75.38			0.25
	5	75.25			0.25

TABLE III: Peak positions and widths of the Xe $4d$ lines in Xe, XeF₂, XeF₄ and XeF₆. *Abbreviation of labels* – Cmpd.: compound, IP_{exp} : experimental peak position, IP_{ADC} : calculated peak position, IP_{rel} : calculated peak position with relativistic correction, Γ_{exp} : experimental peak width. IP_{exp} and Γ_{exp} are photoelectron experimental data, reproduced from table 1 in Ref. 21. For XeF₆ the data with an experimental resolution of 0.11 eV are taken. The values in brackets are the standard deviations of the peak positions and peak widths²¹. IP_{ADC} and IP_{rel} are sorted descending in energy for each compound. The value of IP_{exp} does not necessarily correspond to the values of IP_{ADC} and IP_{rel} in the same row as spin-orbit splitting is neglected to obtain the latter ones. The IP_{ADC} of XeF₆ are the two main peaks in figure 7. All data are given in electronvolt.

The Xe $4d$ and F $2s$ lines in figure 7 are shifted to higher IPs with an increasing number of fluorine atoms (subsection V A 1). This general trend, seen in the mean field approximation of figure 6, can still be identified if electron correlation is taken into account. Nevertheless, the difference between the shifts of the Xe $4d$ lines of XeF₂ and XeF₄ is larger than that between the Xe $4d$ lines of XeF₄ and XeF₆. Electron correlation reduces the effect caused by charge depletion on the xenon atom.

The calculated non-relativistic IPs are listed in table III together with the values obtained by applying the relativistic corrections of section IV. The number of distinct Xe $4d$ lines is smaller in the non-relativistic spectra due to a higher degeneracy caused by neglecting the spin-orbit coupling. The Xe $4d$ lines of XeF₆ cannot be identified clearly in figure 7. One expects from subsection V A 1 two lines for a ground state geometry of O_h symmetry and three lines for a ground state geometry of C_{3v} symmetry. The two IPs, in the energy range of the Xe $4d$ lines of XeF₆ (80–83 eV), with maximum pole

Compound	1 st Experimental IP	1 st ADC IP
Xe	12.129	12.16
XeF ₂	12.35	12.76
XeF ₄	13.1	13.07
XeF ₆	12.35	12.56

TABLE IV: Comparison of the calculated lowest (first) IPs of Xe, XeF₂, XeF₄ and XeF₆ with experimental results. The first IP of xenon is taken from Ref. 54. The other first IPs are taken from Ref. 69. All data are given in electronvolt.

strength are listed in table III.

Adding the relativistic shift $-\Delta\varepsilon$ discussed in section IV to the Xe $4d$ IPs obtained with the help of the ADC(3) programs, the resulting Xe $4d$ IPs differ from the experimentally obtained data in table III only by 1.5–2 eV ($\approx 3\%$) which is a good agreement in view of the complexity of the problem and the necessity to describe the decay simultaneously. The reason for the deviation is twofold. Firstly, the spin-orbit splitting is neglected which amounts to 2.111 eV for the $4d$ lines of the xenon atom, according to section IV. Secondly, since the calculations use ADC(3) for the xenon fluorides, the $3h2p$ -configurations are neglected (ADC(4) calculations are currently beyond reach). The inclusion of these additional configurations would shift the IPs of the Xe $4d$ lines further to lower energy, due to improved hole relaxation⁴⁴, which would cause a considerable improvement.

The first IPs of xenon and its fluorides are compared to the experimental results in table IV. The agreement of experimental IPs and calculated IPs is good.

B. Double Ionization Spectra

The computed double ionization spectra for the xenon atom, the fluorine molecule and the series XeF_{*n*} are shown in figure 8. The ADC $2h$ -pole strength plotted in this figure has a similar meaning as the $1h$ -pole strength for IPs: it characterizes how well the dicationic states are described by $2h$ configurations (subsection III A). The deviation of the $2h$ -pole strength from unity yields the total contribution of $3h1p$ -configurations to the state in question. In analogy to the single ionization spectra, electronically decaying states may also appear in the double ionization spectra^{14,16}. Owing to the discrete basis set used their appearance mimics a discretized Lorentzian curve¹⁶. Such curves may indeed be identified above 50 eV in figure 8 for XeF_{*n*}. The triple ionization threshold of the xenon atom⁷⁰ is 66.2 eV. Short lived states of the cations decay to dications by emitting an electron and similarly such states of the dications decay to trications. The decaying states of the dications must, of course, lie above the triple ionization threshold. Interestingly, the Xe $4d$ lines in the single ionization spectra of the xenon fluorides shown in figure 7 are thus likely to be

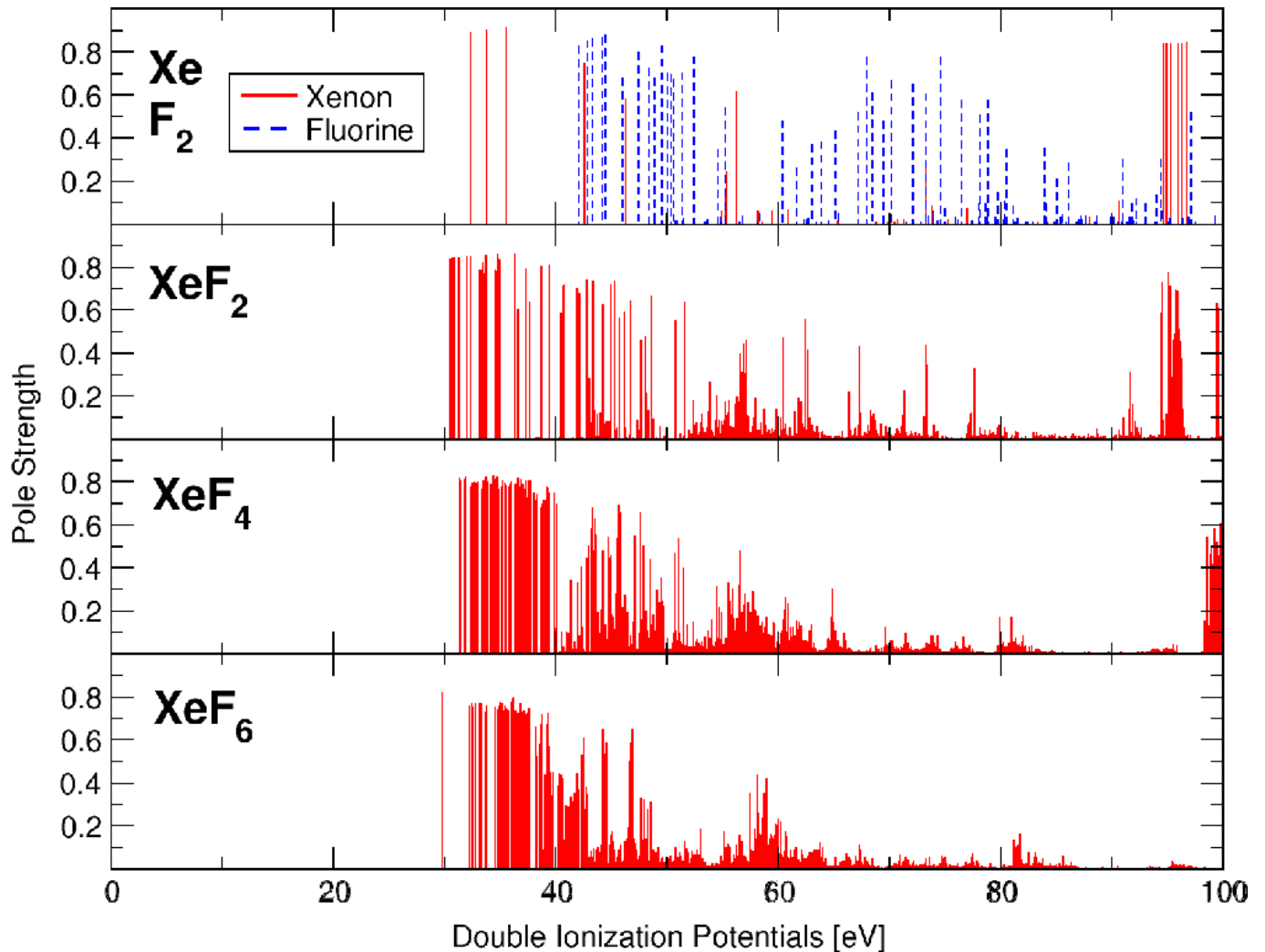


FIG. 8: (Color) Double ionization spectra of Xe, F₂, XeF₂, XeF₄ and XeF₆. The two-particle ADC(2) $2h$ -pole strength is plotted on the ordinate to characterize how well the dicationic final states are described by $2h$ -configurations.

above the triple ionization threshold. This indicates that there is some probability for the Xe $4d$ holes to decay by emitting *two* electrons.

The double ionization spectra in figure 8 comprise ionization out of the outer and the inner valence of Xe, F₂ and XeF_{*n*} because below 80 eV double ionization involving the Xe $4d$ orbitals is energetically impossible. Double ionization from the outer valence of the xenon atom takes place between 30 eV and 40 eV and three distinct DIPs are found in figure 8. The spectra of XeF_{*n*} show in this region increasingly dense lying DIPs which is attributed to a (with the number of fluorine atoms) growing number of outer valence states due to a higher delocalization of the two final state holes. The double ionization spectrum of F₂ in figure 8 shows outer valence ionization of F₂ in the range 40 eV and 55 eV. The general trend in the spectra is a decrease of the validity of the two-hole description of dicationic states of XeF_{*n*} with DIPs above 40 eV with increasing *n*. As all fluorine atoms

in XeF_{*n*} are equivalent (the double ionization spectrum of XeF₆ is obtained in O_h symmetry) dicationic states of the type a hole on xenon and a hole on a fluorine atom are in fact a linear combination of the configurations involving a hole on xenon and a hole on the *n*-th fluorine atom. The coefficients of the linear combinations are determined by the strength of the interaction between the fluorine atoms in XeF_{*n*} being the weakest in XeF₂.

The analysis of the DIPs is more involved than the analysis of the IPs because one has to keep in mind that there are essentially four contributions to a dicationic state which determine its character. The two holes in the dicationic state can be localized on *one* atom, Xe or F, or on *two* different atoms, Xe and F or two different F atoms. The one-site states have a large dicationic population number on either xenon Xe⁻² or on a single fluorine F⁻² and the two-site states are of either Xe⁻¹F⁻¹ or of F₁⁻¹F₂⁻¹ character. For each dicationic state appearing in the spectra of the xenon fluorides, the data of

the population analysis for equivalent fluorine atoms are summed up to yield the population numbers. For example, the $\text{Xe}^{-1}\text{F1}^{-1}$, $\text{Xe}^{-1}\text{F2}^{-1}$ population numbers are added in XeF_2 to give a single $\text{Xe}^{-1}\text{F}^{-1}$ contribution for each dicationic state of the spectrum of XeF_2 . The population numbers are normalized, i.e. the sum of the contributions of Xe^{-2} , F^{-2} , $\text{Xe}^{-1}\text{F}^{-1}$ and $\text{F1}^{-1}\text{F2}^{-1}$ character yields one for each state.

C. One-site Population Numbers

The one-site population numbers are plotted in figure 9 for the xenon fluorides. The spectra are compared to study the effect of the increasing number of fluorine atoms. The first states in the double ionization spectra possess DIPs of ≈ 30 eV. The major contribution of the one-site population Xe^{-2} is at the lower energy part of the spectrum. Obviously, the density of states with a considerable F^{-2} population increases due to the increasing number of fluorine atoms. The overall distribution of these states does not change much in the different compounds, certain regions are visible where the states have a high F^{-2} population. These regions shift slightly to higher DIPs due to the reduced excess charge that the individual fluorine atoms have acquired from the central xenon atom in the ground state of the molecule (see table II).

Conversely, the importance of Xe^{-2} contributions to the dicationic states is extremely reduced due to the reduction of the valence electron density on the xenon atom. In XeF_6 the contributions of Xe^{-2} character have nearly vanished.

D. Two-site Population Numbers

The two-site population numbers for the xenon fluorides are plotted in figure 10. The impact of the increasing number of fluorine atoms is seen here as well. The states with a large $\text{F1}^{-1}\text{F2}^{-1}$ population in the spectrum of XeF_2 are clearly separated into distinct groups of lines originating from $\text{F1 } 2p^{-1} \text{F2 } 2p^{-1}$, $\text{F1 } 2p^{-1} \text{F2 } 2s^{-1}$ and $\text{F1 } 2s^{-1} \text{F2 } 2s^{-1}$ populations. This can be concluded from a simple energy consideration. The IPs in figure 6 for ionization from molecular orbitals with $\text{F } 2p$ character are located at ≈ 20 eV, those for ionization from molecular orbitals with $\text{F } 2s$ character are located at ≈ 40 eV. In the spectrum of XeF_2 in figure 10, the groups are approximately at 40, 60 and 80 eV. Since XeF_2 is a linear molecule, the two fluorine atoms are separated by the central xenon atom. Such states with a large $\text{F1}^{-1}\text{F2}^{-1}$ population are termed *opposite $\text{F1}^{-1}\text{F2}^{-1}$ states*.

The situation changes in XeF_4 and XeF_6 . There are *adjacent* and *opposite $\text{F1}^{-1}\text{F2}^{-1}$ states* and the clear separation between the groups seen in the spectrum of XeF_2 is lost. One reason for this effect is the interaction be-

tween adjacent fluorine atoms which is stronger than the interaction between opposite ones. This leads to a splitting of the fluorine lines which is also observed in the single ionization spectra (subsection V A).

The F1-F2 distance in adjacent $\text{F1}^{-1}\text{F2}^{-1}$ states is considerably reduced in comparison to the F1-F2 distance in opposite states and the hole-hole repulsion energy varies accordingly. Of course, one has to compare states which have a large $\text{F1}^{-1}\text{F2}^{-1}$ population that arises from the same types of orbitals. Therefore, such $\text{F1}^{-1}\text{F2}^{-1}$ states are distributed to a small IP-range in the double ionization spectrum. Corresponding lines in XeF_2 mark the lower ends of such IP-ranges due to the maximum distance between the vacancies therein, in contrast to XeF_4 and XeF_6 .

States with a large $\text{Xe}^{-1}\text{F}^{-1}$ population do not group like those of $\text{F1}^{-1}\text{F2}^{-1}$ character. The density of these $\text{Xe}^{-1}\text{F}^{-1}$ states also increases with an increasing number of fluorine atoms but they are distributed more uniformly over the whole spectral range. In XeF_2 and XeF_6 these states are dominant with respect to population number and in XeF_4 they are comparable to the $\text{F1}^{-1}\text{F2}^{-1}$ states. The DIPs, of the $\text{Xe}^{-1}\text{F}^{-1}$ states are not subject to a change of the hole-hole repulsion energy in contrast to those of the $\text{F1}^{-1}\text{F2}^{-1}$ states because the Xe-F distance does not change within a molecule (remember that the double ionization spectrum of XeF_6 was calculated using octahedral symmetry).

E. Xe 4d Line Width

The increase of the decay width in figure 1 is not very large. If interatomic decay processes become dominant in XeF_n one might expect naively that this leads to a pronounced rise in the decay width with growing n because a multitude of additional decay channels is opened. If this was the case, interatomic electronic decay would have been discovered long ago. Hence there is another discriminating factor for the total Auger decay rate: the transition matrix element in (15). This matrix element depends strongly on the overlap of the initial and final state wave functions. As atomic wave functions decay exponentially with respect to the distance to their center, it is not surprising that the intra-atomic matrix elements are considerably larger than interatomic ones⁶. For an Auger decay that involves the decay of a core hole into two highly localized (core, inner valence) final state holes on the atom that carries the initial vacancy within the molecule, the interatomic matrix elements are exceedingly small. The chemical environment, too, has only a minimal effect.

The electronic decay processes presented in section II are characterized according to their final state population in subsection III C. Using relation (15), the analysis of the final state population numbers in figures 9, 10 shows which of the processes described in section II are important for the electronic decay of $\text{Xe } 4d$ holes in the xenon

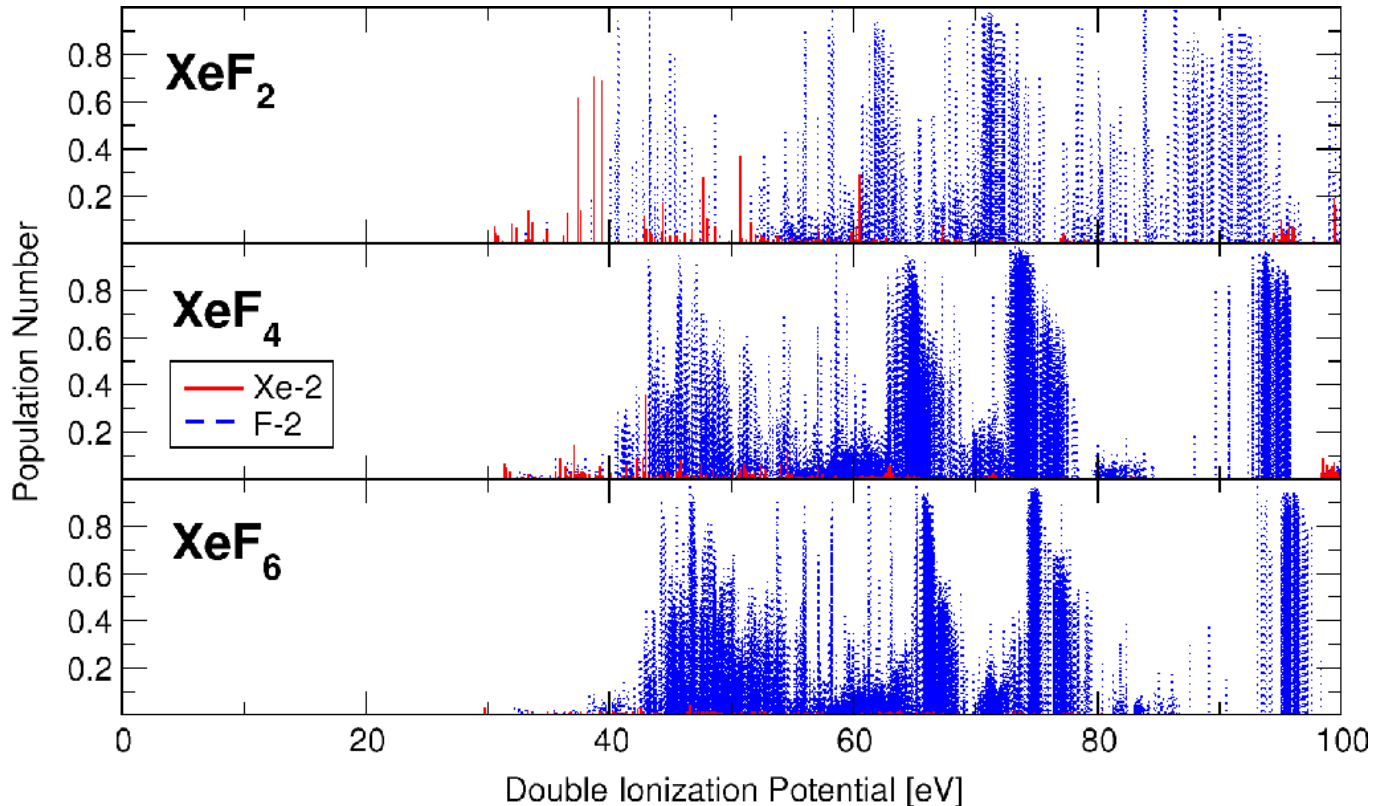


FIG. 9: (Color) One-site population numbers of the double ionization spectra of XeF_2 , XeF_4 and XeF_6 . Each line shown is related to a dicationic state in the double ionization spectra in figure 8. The height of the line gives the one-site population number. Note that the contributions on xenon decrease as the number of fluorine atoms increases.

fluorides.

The intra-atomic electronic decay of an initial $\text{Xe } 4d$ hole produces final states of Xe^{-2} type. The one-site population numbers plotted in figure 9 show that the Xe^{-2} population is extremely low in the xenon fluorides. According to relation (15) the partial decay rate of each cationic state which decays into a given dicationic state can be viewed as a product of an averaged Coulomb matrix element and a two-hole population^{8,23} factor related to the latter state. Hence, as far as population numbers are concerned intra-atomic decay is suppressed and interatomic decay processes dominate the electronic decay of $\text{Xe } 4d$ holes.

Final states with large F^{-2} , $\text{F}_1^{-1}\text{F}_2^{-1}$ population numbers are attributed to two- and three-monomer ETMD processes, respectively. As no partial decay widths for the individual processes are calculated and three-monomer ETMD has not been studied so far, one cannot answer the question which of these two processes is more important. ICD produces $\text{Xe}^{-1}\text{F}^{-1}$ final states. Figure 10 shows that the two-site final state population of ICD is comparable to that of three-monomer ETMD. This fact is somewhat surprising because the valence electron density on the xenon atom in the ground state of the molecule is considerably reduced compared to that in the

isolated atom.

The intra-atomic decay matrix elements are much larger than the interatomic ones, due to the larger overlap of the involved wave functions of the initial and final states. Therefore, the suppression of intra-atomic decay by the Xe^{-2} population numbers of the accessible final states may not be large enough to make interatomic decay processes comparable or even dominant. This relevant issue deserves further studies.

As the intra-atomic decay is increasingly suppressed with an increasing number of fluorine atoms this decrease in decay width must be compensated by the increase in interatomic decay width. We are here in a situation where two competing effects are present which tend to cancel. This is a reason why the significance of interatomic Auger processes is hard to discover. As intra-atomic decay is energetically not possible in inner valence ionized clusters, such clusters are well-suited to study interatomic electronic decay processes. The analogy of Auger decay to the decay of inner valence ionized clusters can then be exploited, as pursued in this article, to identify the impact of interatomic decay processes.

Our analysis suggests that the experimentally observed increase in line width is caused by an increase of the electronic decay width. The conclusion is in contrast to con-

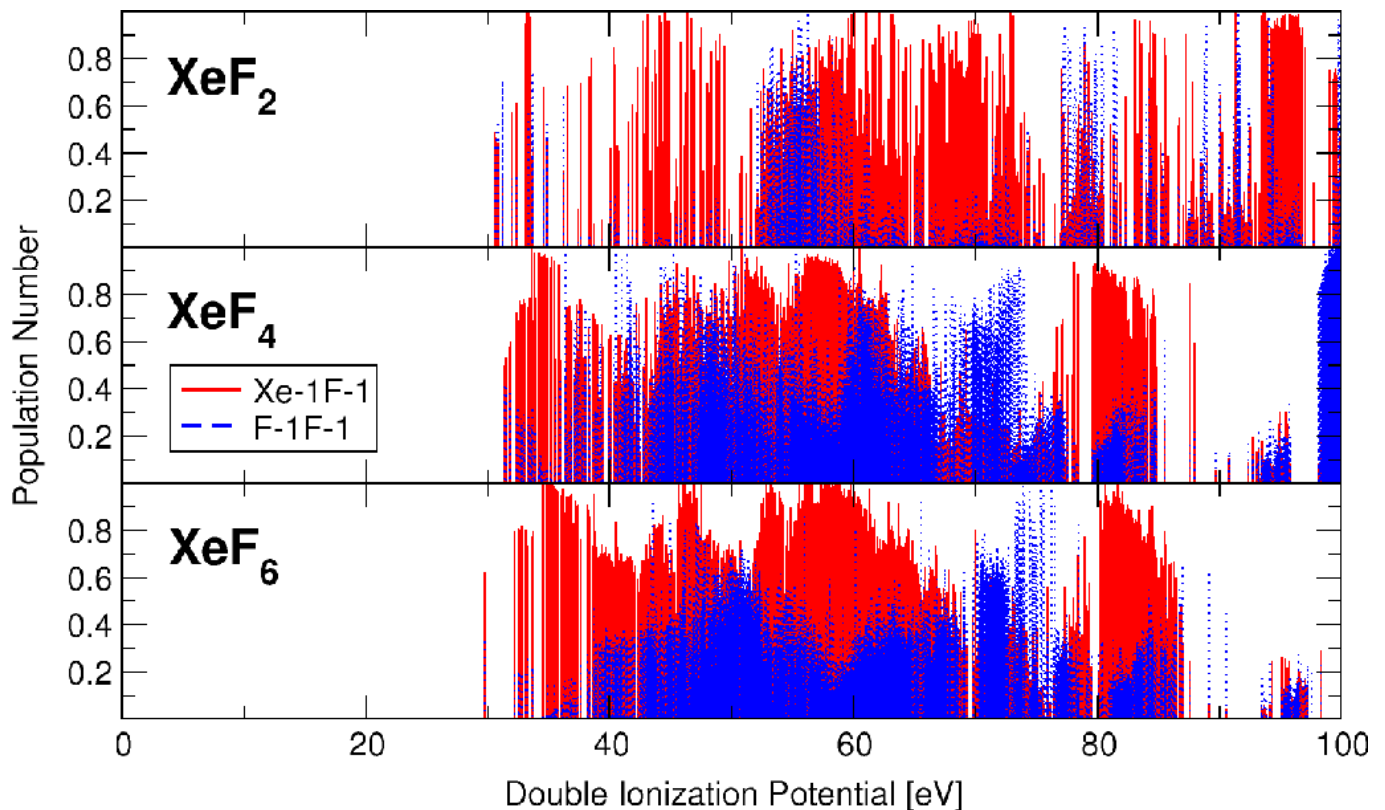


FIG. 10: (Color) Two-site population of the double ionization spectra of XeF_2 , XeF_4 and XeF_6 .

ventional wisdom that the Auger decay rate in molecules is low for a low valence electron density on the atom that carries the initial vacancy⁶. The interatomic decay processes ICD and ETMD are of central relevance in explaining the decay of Xe $4d$ holes in XeF_n .

VI. CONCLUSION

The Auger effect^{1–5} in molecules has been thought of to be an intra-atomic process. This means that only the molecular orbitals with a high probability amplitude on the atom which carries the initial vacancy are involved. The first study of interatomic Auger decays⁷ was discouraging as the relevance of interatomic decay processes was underestimated⁶. Wormeester *et al.* corrected this view on interatomic Auger decay by showing the relevance of interatomic matrix elements in their calculations⁶. Yet they investigated the impact of interatomic matrix elements on an overall scale without dissection into the physical processes introduced in Ref. 7. Newer investigations suggest that the intra-atomic picture of molecular Auger decay fails severely for certain molecules^{9,10,12}.

Molecular Auger decay and electronic decay of clusters after inner valence ionization differ by the energetic scale of the decay electrons and the energy of the electronic states involved in the decay. Furthermore the binding

energy of molecules is much higher than the binding energy of weakly bound clusters which implies a significant modification of the atomic valence orbitals of atoms contained in a molecule which is not the case for the clusters. The energetic scale is given by the initial ionization of the molecular system which is a core ionization in the case of Auger decay and an inner valence ionization in the case of weakly bound clusters. The electronic decay in weakly bound clusters has been studied extensively to elucidate the role of interatomic electronic decay processes. It was discovered that *interatomic Coulombic decay* (ICD)^{14–19} and *electron transfer mediated decay* (ETMD)¹⁷ are efficient interatomic electronic decay processes. The study of weakly bound clusters is simplified by the fact that no intra-atomic electronic decay is possible because the isolated singly ionized monomer is below the double ionization threshold. In molecular Auger decay this is not the case and the identification and the study of interatomic electronic decay processes is by far more complicated.

The analogy to the electronic decay of inner valence ionized weakly bound clusters is therefore employed throughout this article. In first place we discuss the foreign imaging phenomenon^{9–12} discovered in the molecular Auger decay of $2p$ -ionized SiF_4 in terms of ICD and ETMD. This discussion delivers a lucid explanation of this phenomenon. The formally proposed three-monomer ETMD¹⁷ process turns out to be crucial in our

explanation.

To identify the impact of interatomic Auger processes on a thorough basis it is necessary to obtain an estimate of their contribution to the lifetimes of the decaying states at least qualitatively. To this end, Wigner-Weisskopf theory^{24,25} for ionized molecules^{17,19} is extended to include the many-body Green’s function description^{38–40} of dicationic states in the ADC scheme³⁷. With the help of this, a relation between the population numbers of dicationic final states^{8,23} and the electronic decay width could be derived.

Xenon fluorides (XeF_n , $n = 2, 4, 6$) are studied as an example for molecular Auger decay. This family of compounds is chosen due to the experimental observation that the Xe $4d$ line width increases with increasing number of fluorine atoms^{21,22}. We investigate whether this effect arises due to an increase in electronic decay width. The impact on the decay width of interatomic decay processes, which are essential in the decay of weakly bound clusters^{14–19}, is estimated in the xenon fluorides, because their partial decay width increases with an increasing number of fluorine atoms. Xenon is a fairly heavy atom, so relativistic effects^{60,61} have a considerable impact on the ionization potentials of the xenon fluorides. As the theory employed here is strictly non-relativistic, a rule of thumb is devised to correct for the scalar relativistic effects, i.e. the modification of the orbital energies, by performing numeric Hartree-Fock⁵⁹ and Dirac-Fock^{62,63} calculations for the xenon atom. The difference of the orbital energies is used to correct for these effects in XeF_n .

Mulliken and Löwdin population analyses^{33,65} are carried out for XeF_n which show that a considerable amount of charge is withdrawn from the central xenon atom to the fluorine atoms. The effect increases with an increasing number of fluorine atoms. This reduction of charge on the xenon atom leads to a shift of the IPs of xenon in the xenon fluorides to higher energies because the nuclear charge is less effectively screened by the valence electrons.

The ionization spectra are examined on the Hartree-Fock level (Koopmans’ theorem^{33,64}) first because the mean field approximation yields clear and easy-to-understand spectra. The ionization spectra change remarkably when electron correlation is taken into account^{38–40}. The spectra show breakdown of the molecular orbital picture of ionization⁶⁶ in the inner valence of the xenon fluorides and Lorentzian decay curves of singly ionized states above the double ionization threshold are clearly identified especially for the Xe $4d$ -lines. Electron correlation reduces the effect of the withdrawal of charge on the xenon atom considerably and the ionization potentials are lower in energy with respect to their Hartree-Fock values.

To investigate singly ionized electronically decaying states, the double ionization spectra are discussed in terms of the one-site population numbers Xe^{-2} , F^{-2} and two-site population numbers $\text{Xe}^{-1}\text{F}^{-1}$, $\text{F1}^{-1}\text{F2}^{-1}$ of the dicationic states. Separating these two classes of contributions gives considerable insights if these states are

interpreted as dicationic final states of the electronic decay of a single Xe $4d$ vacancy. The one-site population numbers describe decay by intra-atomic electronic decay and three-monomer ETMD and the two-site population numbers describe decay by ICD and two-monomer ETMD. The analysis of the one- and two-site population numbers further reveals that ICD, two- and three-monomer ETMD are likely the relevant interatomic decay processes because intra-atomic Xe^{-2} states acquire only a minimal population in contrast to the population numbers obtained for ICD and ETMD.

The results of the analysis of the population numbers of the double ionization spectra of the xenon fluorides have considerable impact on the understanding of molecular Auger decay. Up to now, only the phenomenon of foreign imaging^{9–12} and the significance of interatomic matrix elements^{6,7} have been known. With this work a clear identification of the physical decay processes is given and the importance of ICD and ETMD is elucidated. It is argued that there is no simple relation between the decay width in molecular Auger decay and the electron density on the atom that carries the initial vacancy. Instead molecular Auger decay is governed by complex many-body effects that tend to compensate the loss in intra-atomic electronic decay width by an increase in the decay width of interatomic electronic decay processes. The experimentally observed Xe $4d$ decay width increases only slightly with an increasing number of fluorine atoms. This can be explained by the vast rise¹⁹ with n of the number of accessible interatomic dicationic final states for Xe $4d$ -ionized XeF_n which prevails in the end over the reduction in intra-atomic electronic decay. This conclusion is in contrast to conventional wisdom that the Auger decay rate in molecules is low for a low valence electron density on the atom that carries the initial vacancy⁶.

Two objections can be made to the arguments presented before: firstly, final state holes in outer valence molecular orbitals are not highly localized, in contrast to holes in inner valence and core orbitals. Hence the picture of one-site and two-site final state holes is only a crude approximation. The Mulliken style population analysis employed sums the contribution of the basis functions of a specific atom in a molecule. So it yields a large population number on a specific atom if a hole in a molecular orbital has a high probability amplitude near the specific atom. If the basis set is reasonable then the Mulliken population analysis yields some sort of dissection of the electron density into point charges. Therefore the picture of one- and two-site holes is replaced by the weaker point charge argument which does not contradict our conclusion that interatomic decay processes are important for the electronic decay of the Xe $4d$ holes. Secondly, the overlap between initial and final state wave functions is large if the final state holes are not very localized. This suggests that quite delocalized final state holes may cause the interatomic matrix elements to become relevant.

Several questions are left open and should be investi-

gated in subsequent work. The three-monomer electron transfer mediated decay is suggested to be an important process to explain the foreign imaging^{9–12} phenomenon (subsection IID) observed in SiF₄ and is addressed in the context of the xenon fluorides. Therefore, it is highly desirable to study this process in a cluster like NeAr₂ as proposed in Ref. 17. Particularly the decay width of this process in relation to interatomic Coulombic decay and two-monomer ETMD is relevant and can have considerable impact on the understanding of interatomic decay processes and their effects.

The F 2*s* states in figure 7 were not examined in this work but are for themselves interesting as they are above the double ionization threshold and consequently can decay. Therefore a detailed study should investigate the effect of interatomic Auger transitions for F 2*s* states in the xenon fluorides. The advantage of studying F 2*s* states are the much slower decay electrons which may enable the precise theoretical determination of their lifetimes.

The accurate determination of lifetimes of electronic resonances is still a problem with *ab initio* calculations²⁸. Standard Gaussian basis sets are optimized to represent compact ground state wave functions of molecules. Hence they are less suited to represent decay electrons further away from the molecule. The situation can be remedied somewhat by augmenting the basis set with a few diffuse functions²⁸, i.e. Gaussians with a small exponent. This

cannot be done excessively because (near) linear dependencies and consequently numerical instabilities arise²⁸. Furthermore basis sets become too large for the expensive calculations. Therefore, new types of basis functions are needed that are capable of representing decay electrons, not only in the vicinity of a molecule. A practical requirement is that it should be possible to evaluate the integrals efficiently which are needed in the Hartree-Fock calculations²⁸. Then it would be possible to determine the lifetimes of the Xe 4*d* vacancies in the xenon fluorides by purely theoretical means.

Acknowledgments

The authors are highly indebted to T. Darrah Thomas for pointing out Ref. 21 to them and supporting it further with valuable private communications (figure 1). Markus Pernpointner helped to estimate the impact of the relativistic effects in the xenon atom. This work would not have been possible without the ADC programs and support by Francesco Tarantelli. Imke B. Müller, Sven Feuerbacher and Thomas Sommerfeld accompanied our work with helpful comments and fruitful discussions. R. S. and L. S. C. gratefully acknowledge financial support by the Deutsche Forschungsgemeinschaft (DFG).

* Corresponding author: Christian.Buth@Post.de;
Present address: Max-Planck-Institut für Physik komplexer Systeme, Nöthnitzer Straße 38, 01187 Dresden, Germany

† Present address: Joint Institute for Laboratory Astrophysics (JILA), University of Colorado, Boulder, CO 80309-0440

¹ P. Auger, *Compt. Rend. (Paris)* **177**, 169 (1923).

² E. H. Burhop, ed., *The Auger Effect and Other Radiationless Transition*, Cambridge Monographs on Physics (Krieger Publishing Company, Melbourne, 1980), ISBN 0-88275-966-3, reprint.

³ M. Thompson, M. D. Baker, J. F. Tyson, and A. Christie, *Auger Electron Spectroscopy*, Chemical Analysis Monographs (John Wiley & Sons, New York, 1985), ISBN 0-471-04377-X.

⁴ W. Bambynek, B. Crasemann, R. W. Fink, H. U. Freund, H. Mark, C. D. Swift, R. E. Price, and P. V. Rao, *Rev. Mod. Phys.* **44**, 716 (1972).

⁵ W. Bambynek, B. Crasemann, R. W. Fink, H. U. Freund, H. Mark, C. D. Swift, R. E. Price, and P. V. Rao, *Rev. Mod. Phys.* **46**, 853 (1974).

⁶ H. Wormeester, H. J. Borg, and A. v. Silfhout, *Surf. Sci.* **258**, 197 (1991).

⁷ J. A. D. Matthew and Y. Komminos, *Surf. Sci.* **53**, 716 (1975).

⁸ F. Tarantelli, A. Sgamellotti, and L. S. Cederbaum, *J. Chem. Phys.* **94**, 523 (1991).

⁹ F. Tarantelli and L. S. Cederbaum, *Phys. Rev. Lett.* **71**, 649 (1993).

¹⁰ F. O. Gottfried, L. S. Cederbaum, and F. Tarantelli, *Phys. Rev. A* **53**, 2118 (1996).

¹¹ T. X. Carroll, K. J. Børve, L. J. Sæthre, J. D. Bozek, E. Kukk, J. A. Hahne, and T. D. Thomas, *J. Chem. Phys.* **116**, 10221 (2002).

¹² T. D. Thomas, C. Miron, K. Wiesner, P. Morin, T. X. Carroll, and L. J. Sæthre, *Phys. Rev. Lett.* **89**, 223001 (2002).

¹³ *Science* **271**, 920 (1996), special issue on clusters.

¹⁴ L. S. Cederbaum, J. Zobeley, and F. Tarantelli, *Phys. Rev. Lett.* **79**, 4778 (1997).

¹⁵ R. Santra, J. Zobeley, L. S. Cederbaum, and N. Moiseyev, *Phys. Rev. Lett.* **85**, 4490 (2000).

¹⁶ J. Zobeley, L. S. Cederbaum, and F. Tarantelli, *J. Chem. Phys.* **108**, 9737 (1998).

¹⁷ J. Zobeley, R. Santra, and L. S. Cederbaum, *J. Chem. Phys.* **115**, 5076 (2001).

¹⁸ R. Santra, J. Zobeley, L. S. Cederbaum, and F. Tarantelli, *J. Electron Spectrosc. Relat. Phenom.* **114-116**, 41 (2001).

¹⁹ R. Santra, J. Zobeley, and L. S. Cederbaum, *Phys. Rev. B* **64**, 245104 (2001).

²⁰ S. Marburger, O. Kugeler, U. Hergenbahn, and T. Möller, submitted.

²¹ J. N. Cutler, G. N. Bancroft, J. D. Bozek, K. H. Tan, and G. J. Schrobilgen, *J. Am. Chem. Soc.* **113**, 9125 (1991).

²² T. D. Thomas (2002), private communication, based on the data taken from Ref. 21 which is reproduced in table III.

²³ F. Tarantelli, A. Sgamellotti, and L. S. Cederbaum, in *Applied Many-Body Methods in Spectroscopy and Electronic Structure*, edited by D. Mukherjee (Plenum Press, New

- York, 1992), pp. 57–104, ISBN 0-306-44193-4.
- ²⁴ J. J. Sakurai, *Modern Quantum Mechanics* (Addison-Wesley, Reading (Massachusetts), 1994), 2nd ed., ISBN 0-201-53929-2.
- ²⁵ V. F. Weisskopf and E. P. Wigner, *Z. Phys.* **63**, 54 (1930).
- ²⁶ R. Santra and L. S. Cederbaum, *J. Chem. Phys.* **115**, 6853 (2001).
- ²⁷ R. Santra, L. S. Cederbaum, and H.-D. Meyer, *Chem. Phys. Lett.* **303**, 413 (1999).
- ²⁸ R. Santra and L. S. Cederbaum, *Phys. Rep.* **368**, 1 (2002).
- ²⁹ J. Zobeley, L. S. Cederbaum, and F. Tarantelli, *J. Phys. Chem. A* **103**, 11145 (1999).
- ³⁰ S. Scheit, L. S. Cederbaum, and H.-D. Meyer, *J. Chem. Phys.* **118**, 2092 (2003).
- ³¹ R. Santra and L. S. Cederbaum, submitted.
- ³² I. B. Müller, J. Zobeley, and L. S. Cederbaum, *J. Chem. Phys.* **117**, 1085 (2002).
- ³³ A. Szabo and N. S. Ostlund, *Modern Quantum Chemistry: Introduction to Advanced Electronic Structure Theory* (Macmillan, New York, 1982), ISBN 0-02-949710-8.
- ³⁴ R. D. Mattuck, *A Guide to Feynman Diagrams in the Many-Body Problem* (McGraw-Hill, New York, 1976), 2nd ed., ISBN 0-07-040954-4.
- ³⁵ E. K. U. Gross, E. Runge, and O. Heinonen, *Many-Particle Theory* (Adam Hilger, Bristol, 1991), ISBN 0-7503-0155-4.
- ³⁶ A. L. Fetter and J. D. Walecka, *Quantum Theory of Many-Particle Systems*, International Series in Pure and Applied Physics, edited by Leonard I. Schiff (McGraw-Hill, New York, 1971).
- ³⁷ J. Schirmer, *Phys. Rev. A* **26**, 2395 (1982).
- ³⁸ J. Schirmer, L. S. Cederbaum, and O. Walter, *Phys. Rev. A* **28**, 1237 (1983).
- ³⁹ J. Schirmer and A. Barth, *Z. Phys. A* **317**, 267 (1984).
- ⁴⁰ J. Schirmer and G. Angonoa, *J. Chem. Phys.* **91**, 1754 (1989).
- ⁴¹ G. H. Golub and C. F. van Loan, *Matrix Computations* (John Hopkins University Press, Baltimore, 1989), 2nd ed., ISBN 0-8018-3772-3.
- ⁴² C. Lanczos, *J. Res. Nat. Bur. Stand.* **45**, 255 (1950).
- ⁴³ H.-G. Weikert, H.-D. Meyer, L. S. Cederbaum, and F. Tarantelli, *J. Chem. Phys.* **104**, 7122 (1996).
- ⁴⁴ G. Angonoa, O. Walter, and J. Schirmer, *J. Chem. Phys.* **87**, 6789 (1987).
- ⁴⁵ J. Schirmer and A. Thiel, *J. Chem. Phys.* **115**, 10621 (2001).
- ⁴⁶ F. Tarantelli, private communication.
- ⁴⁷ J. Brand and L. S. Cederbaum, *Ann. Phys. (New York)* **252**, 276 (1996).
- ⁴⁸ J. Brand and L. S. Cederbaum, *Phys. Rev. A* **57**, 4311 (1998).
- ⁴⁹ J. Brand and L. S. Cederbaum, *Adv. Quantum Chem.* **38**, 65 (2001).
- ⁵⁰ J. Schirmer, *Phys. Rev. A* **43**, 4647 (1991).
- ⁵¹ F. Mertins and J. Schirmer, *Phys. Rev. A* **53**, 2140 (1996).
- ⁵² F. Mertins, J. Schirmer, and A. Tarantelli, *Phys. Rev. A* **53**, 2153 (1996).
- ⁵³ L. Hedin and J. D. Lee, *J. Electron Spectrosc. Relat. Phenom.* **124**, 289 (2002).
- ⁵⁴ A. E. Holleman, E. Wiberg, and N. Wiberg, *Inorganic Chemistry* (Academic Press, New York, 2001), ISBN 0-123-52651-5.
- ⁵⁵ M. Kaupp, C. van Wüllen, R. Franke, F. Schmitz, and W. Kutzelnigg, *J. Am. Chem. Soc.* **118**, 11939 (1996).
- ⁵⁶ Guest, M. F., GAMESS-UK is a package of ab initio programs written by M. F. Guest, J. H. van Lenthe, J. Kendrick, K. Schoffel, and P. Sherwood, with contributions from R. D. Amos, R. J. Buenker, H. J. J. van Dam, M. Dupuis, N. C. Handy, I. H. Hillier, P. J. Knowles, V. Bonacic-Koutecky, W. von Niessen, R. J. Harrison, A. P. Rendell, V. R. Saunders, A. J. Stone, D. J. Tozer, and A. H. de Vries. The package is derived from the original GAMESS code due to M. Dupuis, D. Spangler and J. Wendoloski, NRCC Software Catalog, Vol. 1, Program No. QG01 (GAMESS), 1980.
- ⁵⁷ N. Godbout, D. R. Salahub, J. Andzelm, and E. Wimmer, *Can. J. Chem.* **70**, 560 (1992).
- ⁵⁸ Feller, David and Schuchardt, Karen, basis sets were obtained from the *Extensible Computational Chemistry Environment Basis Set Database*, Version 5/22/02, as developed and distributed by the Molecular Science Computing Facility, Environmental and Molecular Sciences Laboratory which is part of the Pacific Northwest Laboratory, P.O. Box 999, Richland, Washington 99352, USA, and funded by the U.S. Department of Energy. The Pacific Northwest Laboratory is a multi-program laboratory operated by Battelle Memorial Institute for the U.S. Department of Energy under contract DE-AC06-76RLO 1830. Contact David Feller or Karen Schuchardt for further information.
- ⁵⁹ C. Froese-Fischer, *Comp. Phys. Commun.* **14**, 145 (1978).
- ⁶⁰ K. Balasubramanian, *Relativistic Effects in Chemistry: Theory and Techniques* (John Wiley & Sons, New York, 1997), ISBN 0-471-30400-X.
- ⁶¹ P. Pyykkö, *Chem. Rev.* **88**, 563 (1988).
- ⁶² K. G. Dyall, I. P. Grant, T. Johnson, C., F. A. Parpia, and E. P. Plummer, *Comp. Phys. Commun.* **55**, 425 (1989).
- ⁶³ F. A. Parpia, C. Froese-Fischer, and I. P. Grant, *Comp. Phys. Commun.* **94**, 249 (1996).
- ⁶⁴ T. Koopmans, *Physica* **1**, 104 (1933).
- ⁶⁵ R. S. Mulliken, *J. Chem. Phys.* **23**, 1833 (1955).
- ⁶⁶ L. S. Cederbaum, W. Domcke, J. Schirmer, and W. von Niessen (Wiley, 1986), vol. 65 of *Adv. Chem. Phys.*, pp. 115–159.
- ⁶⁷ C. Buth, Diplomarbeit, Ruprecht-Karls Universität Heidelberg, Theoretische Chemie, Physikalisch-Chemisches Institut, Im Neuenheimer Feld 229, 69120 Heidelberg, Germany (2002), www.ub.uni-heidelberg.de/archiv/3004.
- ⁶⁸ C. Buth, R. Santra, and L. S. Cederbaum, to be published.
- ⁶⁹ U. Nielsen and W. H. E. Schwarz, *Chem. Phys.* **13**, 195 (1976).
- ⁷⁰ D. Mathur and C. Badrinathan, *Phys. Rev. A* **37**, 1033 (1987).